A critical role for heme synthesis and succinate in the regulation of pluripotent states transitions

Damien Detraux[1,2], Marino Caruso[1], Louise Feller[1], Maude Fransolet[1], Sébastien Meurant[1], Julie Mathieu[2,3], Thierry Arnould[1], Patricia Renard[1]*

[1]Laboratory of Biochemistry and Cell Biology (URBC), NAmur Research Institute for LIfe Sciences (NARILIS), University of Namur (UNamur), Namur, Belgium, Namur, Belgium; [2]Institute for Stem Cell and Regenerative Medicine, University of Washington, Seattle, United States; [3]Department of Comparative Medicine, University of Washington, Seattle, United States

Abstract Using embryonic stem cells (ESCs) in regenerative medicine or in disease modeling requires a complete understanding of these cells. Two main distinct developmental states of ESCs have been stabilized in vitro, a naïve pre-implantation stage and a primed post-implantation stage. Based on two recently published CRISPR-Cas9 knockout functional screens, we show here that the exit of the naïve state is impaired upon heme biosynthesis pathway blockade, linked in mESCs to the incapacity to activate MAPK- and TGFβ-dependent signaling pathways after succinate accumulation. In addition, heme synthesis inhibition promotes the acquisition of 2 cell-like cells in a heme-independent manner caused by a mitochondrial succinate accumulation and leakage out of the cell. We further demonstrate that extracellular succinate acts as a paracrine/autocrine signal, able to trigger the 2C-like reprogramming through the activation of its plasma membrane receptor, SUCNR1. Overall, this study unveils a new mechanism underlying the maintenance of pluripotency under the control of heme synthesis.

*For correspondence:
patsy.renard@unamur.be

Editor's evaluation

In their study, Detraux D and colleagues provide compelling evidence demonstrating a role for heme biosynthesis on FGF-ERK and TGF β signalling and exit from naïve pluripotency, and in controlling the 2-cell-like cell state. The observations and conclusions provided by the authors are convincing and potentially relevant in the field of pluripotent cell state transitions.

Introduction

The development and regeneration of an organism are two processes held by stem cells. These cells possess unique features such as an unlimited capacity for self-renewal and the ability to differentiate into various cell types. With their pluripotent phenotype, embryonic stem cells (ESCs) retain the ability to differentiate into all cell types of the embryo. First in mouse (*Martin, 1981*; *Evans and Kaufman, 1981*), then later in human (*Thomson et al., 1998*), two main states of pluripotent stem cells have been described: the naïve ESCs, resembling the inner cell mass (ICM) of the pre-implantation embryo epiblast, and the primed ESCs, mirroring the epiblast of the post-implantation stage. While these cells represent timely close stages in embryo development, they display dramatic differences, such as developmental potential (*Gafni et al., 2013*; *Ware et al., 2014*), epigenetic landscape, X-chromosome inactivation pattern and metabolic activity (*Sperber et al., 2015*; *Theunissen et al., 2016*; *Zhou*

et al., 2012; *Sahakyan et al., 2017*; *Grow et al., 2015*; *Takashima et al., 2014*; *Nichols and Smith, 2009*). Aside from these two pluripotent stages, ESC culture is known to be very heterogenous in terms of pluripotent or epigenetic marker expression (*Sustáčková et al., 2012*). Interestingly, a small population (representing about 1 %) of mouse ESCs grown in naïve conditions displays features of the two-cell stage embryo (2C-like population or 2CLCs) exhibiting extended potential (*Macfarlan et al., 2012*). This subset also displays the expression of 2C-specific genes such as the *Zscan4* cluster, the retro-transposable element *MuERVL* or the master regulator DUX (*Macfarlan et al., 2012*; *Percharde et al., 2018*; *Ishiuchi et al., 2015*), a disappearance of chromocenters and loss of the core pluripotency protein OCT4 (*Macfarlan et al., 2012*). However, despite the well-known differences between the different pluripotent states, little is understood about the molecular mechanisms governing the transition between them.

Several studies have started to address the question of the naïve-to-primed ESC transition using different screening methods to identify genes controlling this transition (reviewed in *Li et al., 2020*). Notably, a few studies have revealed mTORC1/2 as a critical component for the naïve-to-primed transition (*Mathieu et al., 2019*; *Li et al., 2018*; *Duggal et al., 2015*) that regulates key developmental pathways such as Wnt signaling (*Sperber et al., 2015*; *Mathieu et al., 2019*; *Xu et al., 2016*; *Taelman et al., 2019*). Among the hits of the different screens, we observed the recurrence of genes involved in the heme biosynthesis pathway. This pathway, starting in mitochondria, uses succinyl-CoA and glycine as starting material. It then proceeds to successive cytosolic reactions before ending by the formation of the heme molecule in the mitochondrial matrix. Although largely studied in hematopoietic stem cells, the roles of this biosynthetic pathway and this metabolite have never been studied in the context of pluripotency. In this study, we demonstrate the incapacity of mouse ESCs (mESCs) to exit from naïve toward the primed state under heme synthesis inhibition, a process caused by the inability to activate the core MAPK and TGFβ-SMADs signaling pathways due to an accumulation of extramitochondrial succinate. We also show that heme synthesis inhibition in naïve mESCs favors the emergence of 2CLCs in the cell population. This effect is heme-independent as hemin supplementation does not prevent it. We next demonstrate that the reprogramming in 2C-like state upon heme biosynthesis inhibition is actually caused by the accumulation and release of succinate derived from the heme synthesis inhibition, acting as both paracrine and autocrine signals.

Results

Murine ESCs are dependent on heme biosynthesis to properly transition to the primed stage

In order to unveil the pathways required for the naïve-to-primed ESC transition, we compared the results of whole genome CRISPR-Cas9 screens previously published for mouse and human ESCs (*Mathieu et al., 2019*; *Li et al., 2018*). The significant hits (p val <0.05) were submitted to the DAVID functional annotation tools. For the human screen, positive hits for apoptosis were removed. Indeed, since a negative selection was applied to induce the death of primed human ESCs (hESCs), cells that acquired a resistance to cell death by mutating genes involved in apoptosis would be spared. *Figure 1a* displays the top Gene Ontologies (GO) for the DAVID biological processes showing 'heme biosynthetic process' as one of the most enriched in both studies (*Mathieu et al., 2019*; *Li et al., 2018*). Seven out of 8 enzymes of this metabolic pathway (ALAD, PBGD, UROS, UROD, CPOX, PPOX, and FECH) came out as positive hits in the CRISPR screen during the naïve-to-primed mESC transition. In hESCs, only the 4 cytosolic enzymes (PBGD, UROS, UROD, and CPOX) were highlighted. In both models, the expression of these genes both in vitro and in vivo is not modified *Table 1*. Together, the results stress the importance of this metabolic pathway for the naive-to-primed transition, although its role in non-hematopoietic stem cells is poorly understood.

Experimentally, to trigger the exit of the naïve mESC state, the serum-free media with naïve cytokines cocktail (LIF; CHIR99021 and PD0325901; 2iL) is switched to a media with fibroblast growth factor 2 (FGF2) and activin A for 48 hr, allowing mESCs to gain post-implantation features (EpiLC). Using succinylacetone (SA) to inhibit heme synthesis, by interfering with ALAD activity (*Sassa and Kappas, 1983*), and 10 µM of hemin for its rescue, we show that, when mESCs are pushed for 48 hr to exit the naïve stage (EpiLC) in the presence of SA (EpiLC +SA), the expression of the primed gene markers *Fgf5*, *Fgf15*, *Otx2*, *Oct6*, *Dnmt3a*, and *Zic2* is significantly reduced (*Figure 1b*). In addition,
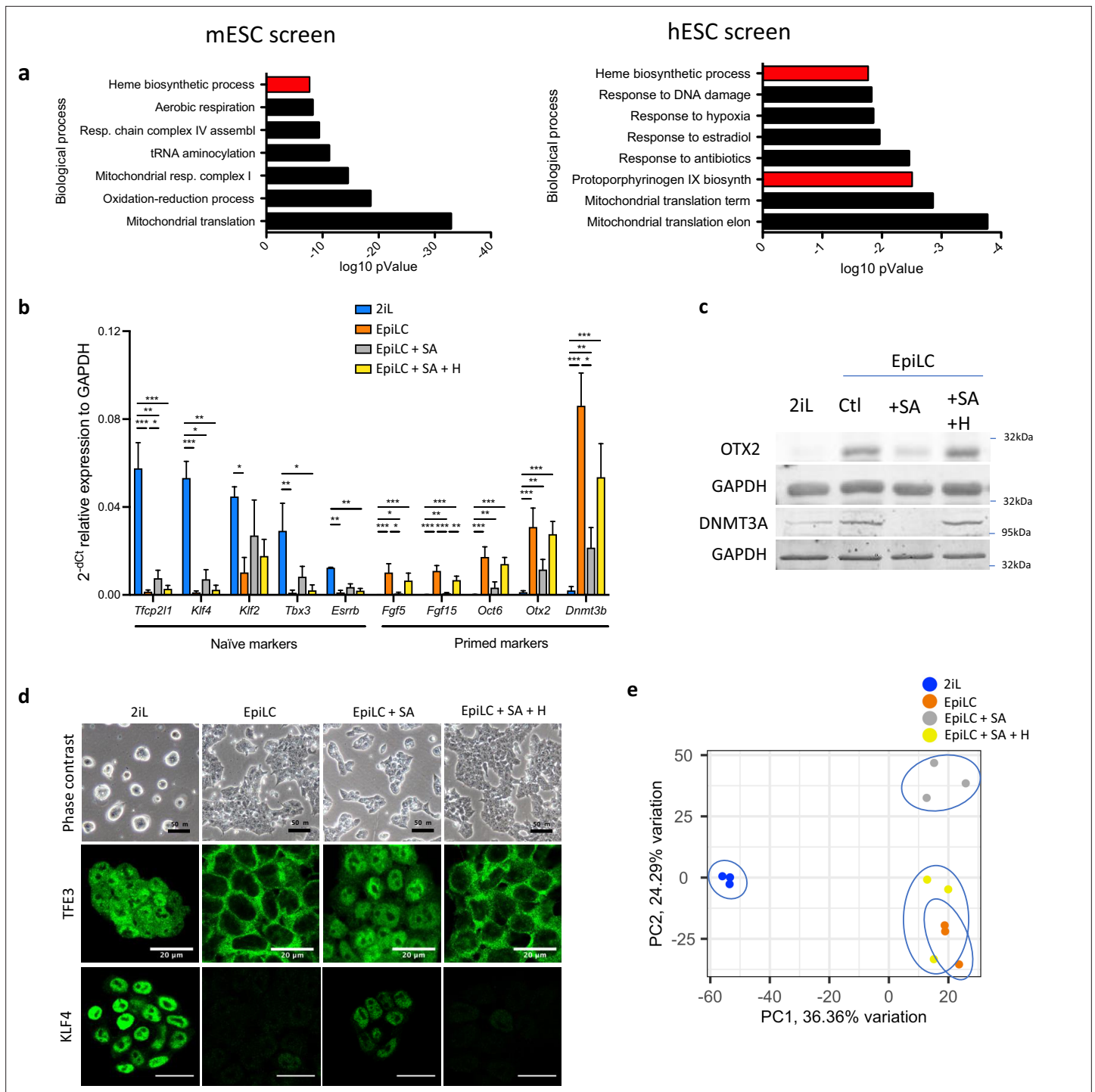
Figure 1. Heme synthesis inhibition impairs the exit of mESCs from the naïve state; effect mediated by heme. (**a**) DAVID biological processes GO enrichment from two independent CRISPR-Cas9 screens for the naive state exit, in mouse (left panel) (**Li et al., 2020**) and in human (right panel) (**Mathieu et al., 2019**). The heme biosynthetic pathway is highlighted In red. (**b**) Relative expression of naïve and primed markers of mESCs in naïve conditions (2iL), in transition for 2 days to the Epi stage (EpiLC) with or without 0.5 mM succinylacetone as heme synthesis inhibitor (EpiLC +SA) and 10 µM hemin supplementation (EpiLC +SA + H), assessed by RT-qPCR relative to *Gapdh* expression (*Tfcp2l1*, transcription factor CP2-like 1; *Esrrβ*, estrogen-related receptor β; *Klf2/4*, Kruppel-like factor 2/4; *Tbx3*, T-Box Transcription Factor 3; *Fgf5/15*, fibroblast growth factor-5/15; *Zic2*, zic family member 2; *Otx2*, homeobox protein 2). Results expressed as mean +/-S.D. *p<0.05, **p<0.01, ***p<0.001. ANOVA-1. n=3 independent biological replicates. (**c**) Western blot analysis of the protein abundance of OTX2 and DNMT3A relative to GAPDH as a loading control for cells in naïve conditions (2iL), in transition for 2 days to the Epi stage (EpiLC) with 0.5 mM SA (+SA) and 10 µM hemin (+H) supplementation. Representative blot of three

Figure 1 continued on next page

Figure 1 continued

biological replicates. (**d**) Phase contrast micrographs of cells in naive (2iL), or in transition to the primed (EpiLC) state with treatment with SA and hemin (**H**). Scale bar = 50 μm. Confocal micrographs of mESCs in naive stage or in transition for TFE3 (Transcription Factor Binding To IGHM Enhancer 3) and KLF4, in green. Scale bar = 20 μm. TFE3 n=3 and KLF4 n=3 biological replicates (**e**) Principal component analysis (PCA) of the normalized RNAseq data transcripts.

The online version of this article includes the following source data and figure supplement(s) for figure 1:

Figure supplement 1. Heme synthesis inhibition perturbs the exit of the naïve state in mESCs and hESCs.

Figure supplement 1—source data 1. Raw uncropped and annotated western blot images for *Figure 1—figure supplement 1c*.

Source data 1. Raw uncropped and annotated western blot images for *Figure 1c*.

the loss of expression for naïve markers (*Esrrb, Tfcp2l1, Klf2-4, and Tbx3*) is partially prevented in these conditions. This was confirmed at the protein level by a decrease in the abundance of OTX2 and DNMT3A analyzed by western blot (*Figure 1c*) and the increase in the abundance of KLF4 by immunofluorescence, when cells were treated with SA during the transition (*Figure 1d*). Furthermore, the subcellular localization of TFE3, mainly nuclear in naïve cells and only cytosolic in primed cells (*Mathieu et al., 2019*; *Betschinger et al., 2013*), remains nuclear in the presence of SA (*Figure 1D*). Hemin supplementation restores the gene expression, the protein abundance and the subcellular localization of TFE3 to levels similar to those found in cells incubated without SA (*Figure 1a–d*). To consolidate this, we then generated an ALAD KO line, which was maintained in culture with hemin supplementation to avoid degeneration. In accordance with the results obtained with SA, removal of hemin during the transition perturbed the exit from the naive state (*Figure 1—figure supplement 1*). Finally, principal component analysis (PCA) of the normalized gene expression from RNA sequencing also reveals the segregation of the cells treated with SA (EpiLC + SA) from either the controls (EpiLC) or the cells rescued with hemin (EpiLC +SA + H) (*Figure 1e*). An impairment of the naïve state exit is also observed to some extent in human ESCs (Elf1 cell line) when pushed to exit in TeSR for 4 days (*Figure 1—figure supplement 1c*). Overall, these results confirm the functional screen data by showing that the inhibition of heme biosynthesis impairs the naive-to-primed mESC transition.

Heme synthesis inhibition prevents the activation of key signaling pathways associated with implantation

Heme deficiency is canonically sensed in mammals through the nuclear factor BACH1 (reviewed in *Zhang et al., 2018*), increasing its nuclear localization or the activation of the integrated stress response (ISR; reviewed in *Pakos-Zebrucka et al., 2016*) through the action of the heme-regulated inhibitor (HRI). While we did not observe an accumulation of BACH1 in the nucleus following SA treatment (*Figure 2—figure supplement 1a*), we did observe an increase in EIF2α phosphorylation and a reduction in global protein translation, both showing activation of the ISR (*Figure 2—figure supplement 1b-c*). However, activation of this pathway with a chemical activator of HRI, BTdCPU (*Chen et al., 2011*), effectively reducing protein translation to the extent of SA, did not prevent the exit from the naive stage (*Figure 2—figure supplement 1d-e*). Thus, to identify the mechanisms involved in the failure of the cells to properly undergo the transition, we performed a gene set enrichment analysis (GSEA) with the KEGG pathways (Kyoto Encyclopedia of Genes and Genomes) between EpiLC and EpiLC +SA RNAseq data. While genes involved in xenobiotic detoxification or cytochrome P450 are expected to be upregulated in response to SA-induced heme deprivation (*Vinchi et al., 2014*; *Lämsä et al., 2012*), many crucial signaling pathways involved in development are shown negatively enriched in SA-treated condition (*Figure 2a*). We thus focused our attention on the pathways directly associated with the naive-to-primed transition that is triggered by the combined presence of FGF2 and activin A in the growth culture medium, especially since detailed analysis of the PC loadings driving the PC2 separation (*Figure 1e*) highlights several SMAD pathway-related proteins (*Figure 2—figure supplement 1f*). On the one hand, the MAPK-ERK1/2 pathway (downstream of FGF2) was not activated in EPI +SA cells, as shown by the absence of phosphorylation of ERK1/2 (*Figure 2—figure supplement 1g*). On the other hand, the activin A-SMAD pathway activation was also compromised as shown by the difference in nuclear localization of SMAD2/3 when compared to the EpiLC cells (*Figure 2—figure supplement 1h*) or SMAD3 phosphorylation (*Figure 2b–c*). Interestingly, chemical inhibition of those two pathways by 1 μM PD0325901 (MEKi) and 5 μM SIS3 (TGFβ-SMADi)

Table 1. Relative expression of heme synthesis enzymes.

(a) Fold change expression of the 8 enzymes of the heme synthesis pathway, based on normalized data from bulk RNAseq or proteomics analysis, extracted from published datasets. (b) Normalized gene expression counts of heme synthesis enzymes from in vivo mouse blastocysts analyzed by RNAseq.

a

Source	Human ESCs				Mouse ESCs	
	Di Stephano et al.		Grow et al.	Sperber et al.	Nakamura et al.	This study
Type	Proteomics	Transcriptomics	Transcriptomics			
ALAS	0,7	0,88	1,22	0,95	0,85	1,016
ALAD	0,47	0,29	0,81	0,96	0,54	0,92
HMBS	1,43	0,84	1,22	1,27	1,15	0,81
UROD	1,12	1,05	0,62	1,10	1,33	0,64
UROS	2,09	1,58	0,78	1,12	0,50	0,75
CPOX	1,24	2,07	1,02	1,25	1,12	0,87
PPOX	2,09	1,54	1,16	1,37	1,25	0,56
FECH	0,98	1,10	1,28	0,77	1,06	1,30

b

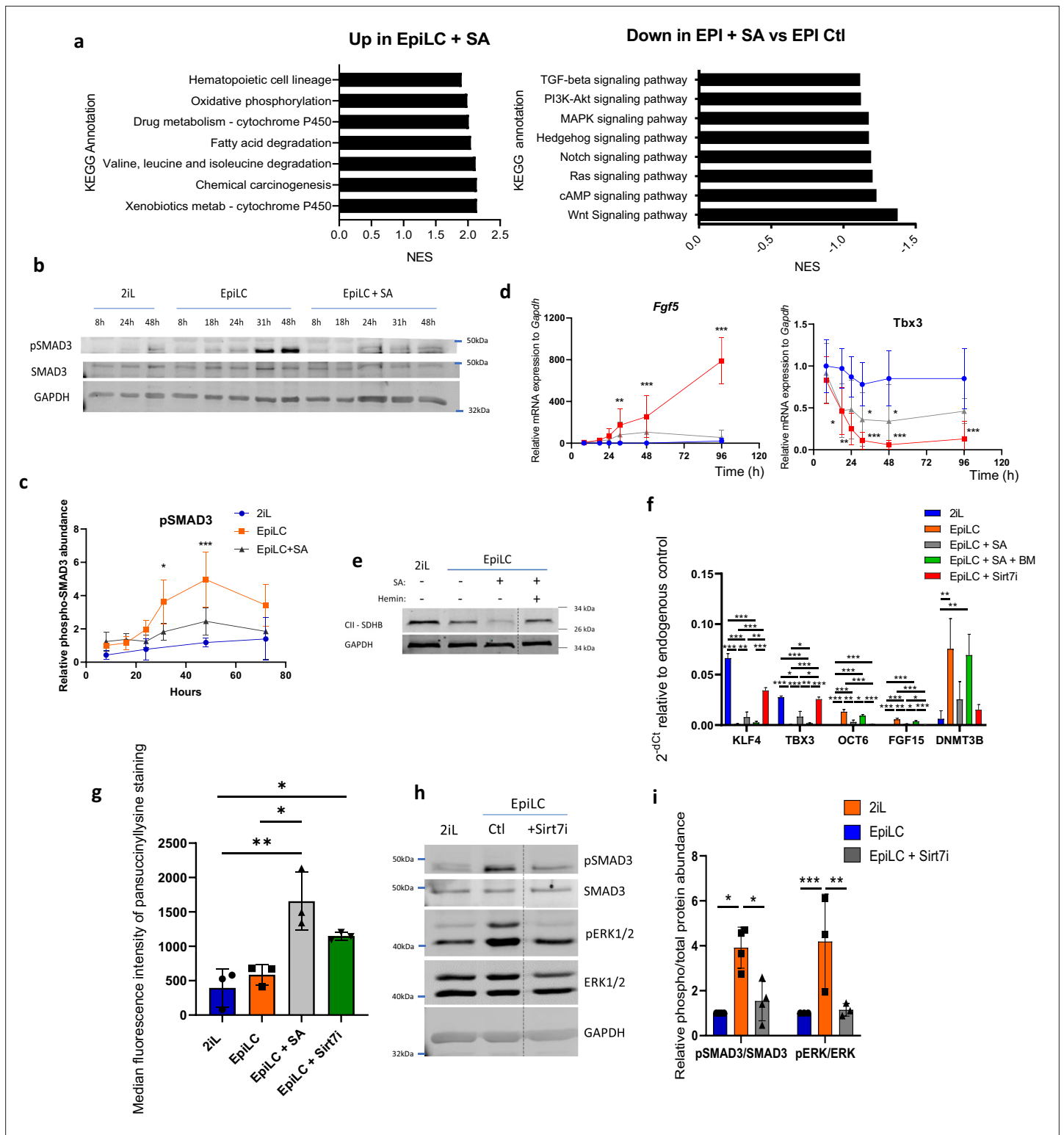|	Mouse blastocysts		
	Nakamura et al.		
Stage	E4.5	E5.5	E6.5
Alas	17	12	16
Alad	40	22	33
Hmbs	73	65	60
Uros	2,2	5,4	5,7
Urod	43	53	80
Cpox	22	13	14
Ppox	14	7	7
Fech	8	26	28

Enzyme

Figure 2. SA prevents the activation of the MAPK and Activin A-SMAD pathways during the mESC transition through the cytosolic accumulation of succinate. (**a**) GSEA performed on RNAseq data were analyzed for KEGG pathways. Up- and Down-regulated KEGG pathways in EpiLC + SA versus EpiLC Ctl, represented as normalized enrichment scores (NES). (**b**) Western blot analysis of the time course protein abundance of SMAD3 and phospho-SMAD3 relative to GAPDH as a loading control for cells in naïve conditions (2iL), in transition for up to 2 days to the Epi stage (EpiLC) with 0.5 mM SA as heme synthesis inhibitor. Representative blot of 5 biological replicates, and quantified in (**c**). (**d**) Time course gene expression analysis of Fgf5 and Tbx3 assessed by RT-qPCR, expressed as mean +/-S.D. ANOVA-2. n=5 independent biological replicates. (**e**) Western blot analysis of SDHB during the

Figure 2 continued on next page

Figure 2 continued

transition, relative to GAPDH as loading control. Representative blot of 2 biological replicates. (**f**) Relative expression of naïve and primed markers of mESCs in naïve conditions (2iL), in transition for 2 days to the Epi stage (EpiLC) with or without 0.5 mM SA (EpiLC + SA), 1 μM butylmalonate (+BM) or 5 μM of Sirt7 inhibitor supplementation, assessed by RT-qPCR relative to *Gapdh* expression. n=3 independent biological replicates. ANOVA1 (**g**) Median fluorescence intensity of succinyllysine residues measured by flow cytometry for mESC in transition with 5 μM Sirt7 inhibitor (Sirt7i). n=3 independent biological replicates, ANOVA1. (**h**) Representative western blot analysis of the abundance of the total and phosphorylated forms of SMAD3 and ERK1/2, using GAPDH as loading control, for mESC in transition with a Sirt7 inhibitor (Sirt7i), and quantified in (**i**).

The online version of this article includes the following source data and figure supplement(s) for figure 2:

Source data 1. Raw uncropped and annotated western blot images for *Figure 2b*.

Source data 2. Raw uncropped and annotated western blot images for *Figure 2e*.

Source data 3. Raw uncropped and annotated western blot images for *Figure 2h*.

Figure supplement 1. SA prevents the activation of the MAPK and Activin A-SMAD pathways during the mESC transition.

Figure supplement 1—source data 1. Raw uncropped and annotated western blot images for *Figure 2—figure supplement 1b*.

Figure supplement 1—source data 2. Raw uncropped and annotated western blot images for *Figure 2—figure supplement 1c*.

Figure supplement 1—source data 3. Raw uncropped and annotated western blot images for *Figure 2—figure supplement 1d*.

Figure supplement 1—source data 4. Raw uncropped and annotated western blot images for *Figure 2—figure supplement 1g*.

(*Figure 2—figure supplement 1g-h*) shows that the inhibition of the SMAD translocation mimics the transition defects observed with SA as revealed by the gene expression analysis of naive and primed markers (*Figure 2—figure supplement 1i*). This pathway inhibition was especially observed after 24 h of treatment, and concomitant with the defect in gene expression (*Figure 2b–d*). Addition of two- or threefold increased doses of activin or FGF2 did not rescue the gene expression pattern, indicating a strong inhibition (*Figure 2—figure supplement 1j*). Mechanistically, previous reports have shown that heme biosynthesis consumes a lot of the glycine and succinyl-CoA precursors in the mitochondria, acting as some sort of 'succinyl-CoA sink' (*Atamna, 2004*). We thus hypothesized that heme synthesis inhibition would increase the abundance of succinyl-CoA in mitochondria, that could then exit the organelle in the form of succinate and accumulate in other cell compartments (*Atamna, 2004*). The accumulation of succinate precursor is reinforced by the observed decreased abundance of the succinate dehydrogenase (SDH), consuming succinate in the TCA, known to be destabilized by the loss of heme (nicely reviewed in *Kim et al., 2012*; *Figure 2e*). Together, these results indicate a possible accumulation of succinate in response to heme synthesis inhibition, that could potentially cause the transition defect. To test this hypothesis, we used butylmalonate (BM), an inhibitor of the dicarboxylate carrier (DIC; SLC25A10), to prevent leakage of succinate from the mitochondrial matrix to the cytosol (*Mills et al., 2018*), and this nicely resumed the transition as shown by the gene expression profile of mESCs in the EpiLC + SA + BM condition (*Figure 2f*).

Succinate accumulation and/or SDH ablation is known to increase protein lysine succinylation (*Smestad et al., 2018*), an effect that is observed upon SA treatment and that we mimicked by inhibiting Sirt7, a cytosolic and nuclear desuccinylase (*Figure 2g*). The ability of this molecule to mimic SA in the pathway's inhibition (*Figure 2h–i*) and to prevent the exit of the naive state (*Figure 2f*) points at succinylation events as the cause of the transition defects.

Blockade of heme synthesis in naive mESCs triggers the activation of a 2C-like program

In addition to this defect in the exit from the naive state, we found that treatment of naïve 2iL cells with SA also modifies the global gene expression as 2iL + SA samples cluster away from 2iL control cells when analyzed by PCA performed on RNAseq data (*Figure 3a*). Our attention was thus drawn on markers reported to be expressed in the two-cell embryo. Indeed, a small proportion of the mESC population actually expresses a gene signature reminiscent of the 2 C stage, these cells thus called 2C-like cells (2CLCs) (*Macfarlan et al., 2012*). Indeed, the expression of the 142 genes previously identified as upregulated in this 2C-like population (*Macfarlan et al., 2012*) was statistically upregulated in 2iL versus 2iL + SA (*Figure 3b*) and this was further confirmed by RT-qPCR for a selection of the most common markers (*Figure 3c*) and further supported by the upregulation of the 2CLC markers in ALAD KO mESCs (*Figure 3d*). As the studies that characterize this 2C-like population
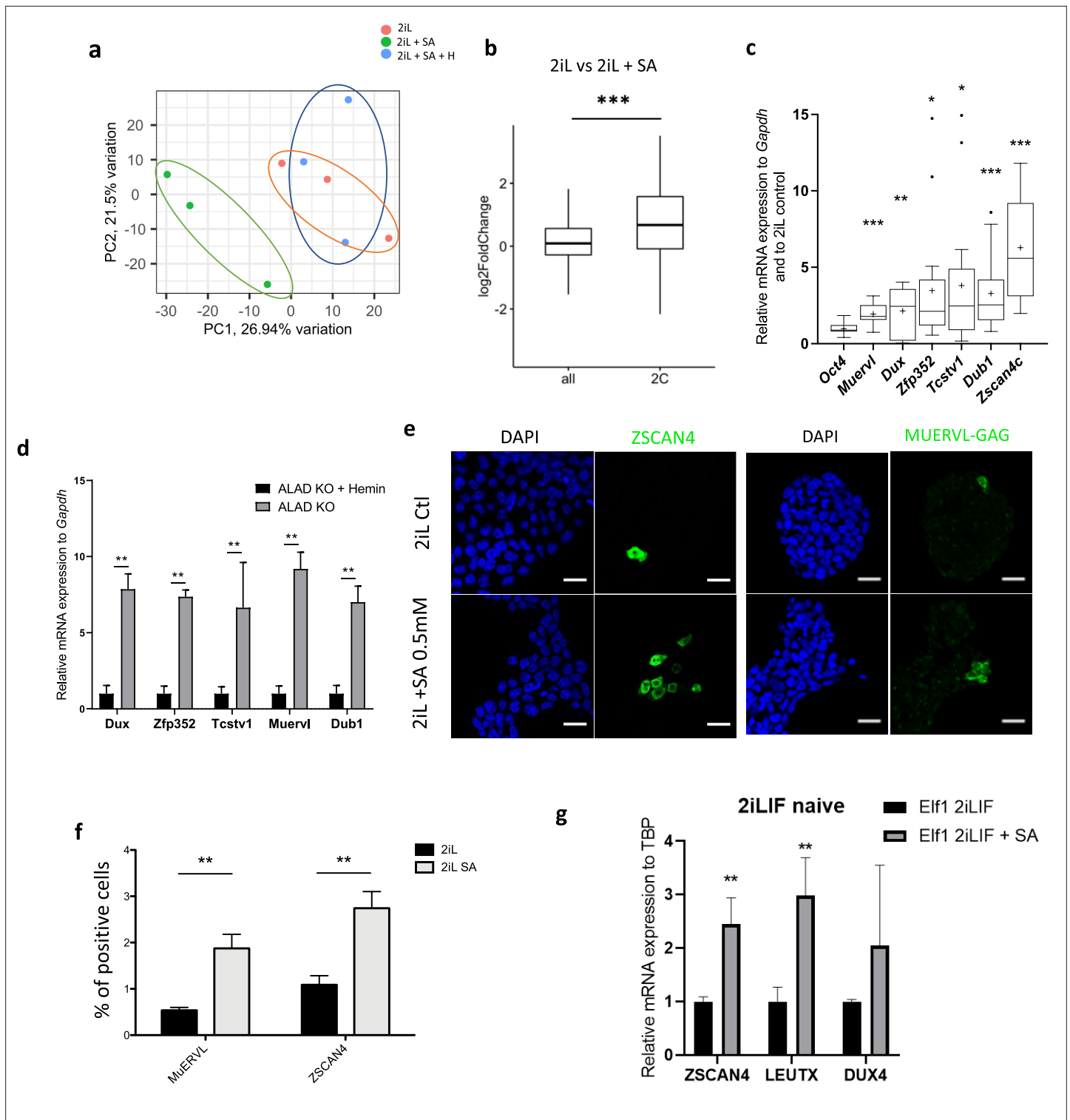
Figure 3. Heme synthesis inhibition pushes mESCs toward a 2C-like stage. (**a**) Principal component analysis (PCA) of the normalized RNAseq data transcripts of naïve mESCs (2iL) treated for 48 hr with 0.5 mM SA ± 10 μM Hemin. (**b**) Boxplot of mean Log2FC of 2 C markers defined in ***Macfarlan et al., 2012*** or all analyzed mRNAs in 2iL +SA versus 2iL control cells. Statistical significance is calculated by Student T-test. p<0.001. (**c**) Relative expression of 2 C gene markers of mESCs assessed by RT-qPCR relative to *Gapdh* expression and to 2iL naïve control represented as a Tukey box and whisker plot. The line represents the median and the +is the mean. *Oct4*=octamer-binding transcription factor 4, Muervl = murine endogenous retrovirus-like, Dux = double homeobox, *Zfp352*=Zinc-finger protein 352, *Tcstv1*=2-cell-stage variable group member 1, *Dub1*=Ubiquitin Specific Peptidase 36, *Zscan4c*=Zinc Finger And SCAN Domain Containing 4, isoform c. n=9. (**d**) Gene expression analysis of 2CLC markers of ALAD KO mESCs

Figure 3 continued on next page

report an important heterogeneity at the population level (*Macfarlan et al., 2012*; *Eckersley-Maslin et al., 2016*), we quantified the fraction of ZSCAN4$^+$ and MUERVL-GAG$^+$ cell populations by immunostaining followed by confocal microscopy observations. As shown in *Figure 3e and f*, treatment with SA increases the fraction of 2C-like cells by two to three folds. A similar trend is observed for genes involved in the ZGA for hESCs (*Taubenschmid-Stowers et al., 2022*; *Figure 3g*).

The induction of the 2C-like program is succinate-dependent

Interestingly, and as opposed to the naive-to-primed setup, the observed phenotype seems independent of heme as it is not rescued by hemin supplementation (*Figure 4a–b*). We thus investigated the putative role of succinate accumulation in the phenotype. The abundance of succinylated proteins in naive cells treated or not with SA was assessed using a pan-succinyllysine antibody in confocal microscopy and in flow cytometry (*Figure 4c*). In basal conditions, the bulk of succinyllysine modifications are located in the mitochondria (*Figure 4—figure supplement 1*), as expected. However, a dramatic increase in the signal associated with succinylated proteins is observed in all subcellular compartments when heme synthesis is inhibited, an effect that is not (or very partially) rescued upon hemin supplementation (*Figure 4c*). We then postulated that blocking the exit of this metabolite from mitochondria would prevent the acquisition of widespread succinyl-lysine post-translational modifications and impair the acquisition of the 2C-like cells markers, only if this phenotype is dependent on increased succinate concentration. As hypothesized, addition of BM combined to SA is correlated to a rescue of both the increase in 2 C markers and the proportion of ZSCAN4 or MUERVL-positive cells in the population (*Figure 4a and d*). Altogether, this shows that an accumulation of extra-mitochondrial succinate upstream of heme synthesis in naive mESCs induces a 2C-like phenotype, reinforced by the inability of glycine to induce same effect (*Figure 4a*). In order to observe the levels of protein succinylation, and by extension the levels of succinate, in endogenous 2CLCs of the mESC population, we took advantage of a previously described reporter cell line for this 2C-state, characterized by the stable insertion of a construct containing a turboGFP-coding gene under the control of the MUERVL long terminal repeat (2 C:::turboGFP; *Ishiuchi et al., 2015*; *Rodriguez-Terrones et al., 2020*). The simultaneous observation of the endogenous GFP fluorescence, the absence of OCT4 (*Macfarlan et al., 2012*) and the immunostaining of the succinyl-lysine residues showed an increase in protein succinylation specifically in the 2C-like cells (GFP+; OCT4-) sub-population, as quantified by flow cytometry (*Figure 4e–f*).

Since we showed that the increase in the reprogramming of some mESCs to a 2C-like state after heme synthesis inhibition was the result of succinate exit from mitochondria, we then aimed to further confirm these results, by inducing a mitochondrial accumulation of succinate, independently of heme biosynthesis inhibition, using Atpenin A5 (AA5), an SDH inhibitor (*Miyadera et al., 2003*). AA5 induces the protein lysine succinylation (*Figure 5a*), an increase in the number of ZSCAN4-positive cells (*Figure 5b*) and the expression of 2 C markers (*Figure 5c and e*). These effects were counteracted by the addition of BM to prevent the succinate exit from the mitochondria (*Figure 5b*), confirming the involvement of succinate in the process.

Succinate acts through the activation of its receptor, SUCNR1, to trigger the 2C-like program

Once in the cytosol, succinate could either inhibit the α-ketoglutarate (αKG)-dependent-dioxygenases or exit the cell through the monocarboxylate transporters (MCTs) and act as an extracellular signal molecule. Indeed, succinate is a reaction product of hydroxylation reactions catalyzed by αKG-dependent dioxygenases. Three families of dioxygenases are known to be sensitive to an increase in succinate concentration: the prolyl-hydroxylases (PDHs), the Ten-eleven translocation (TET)
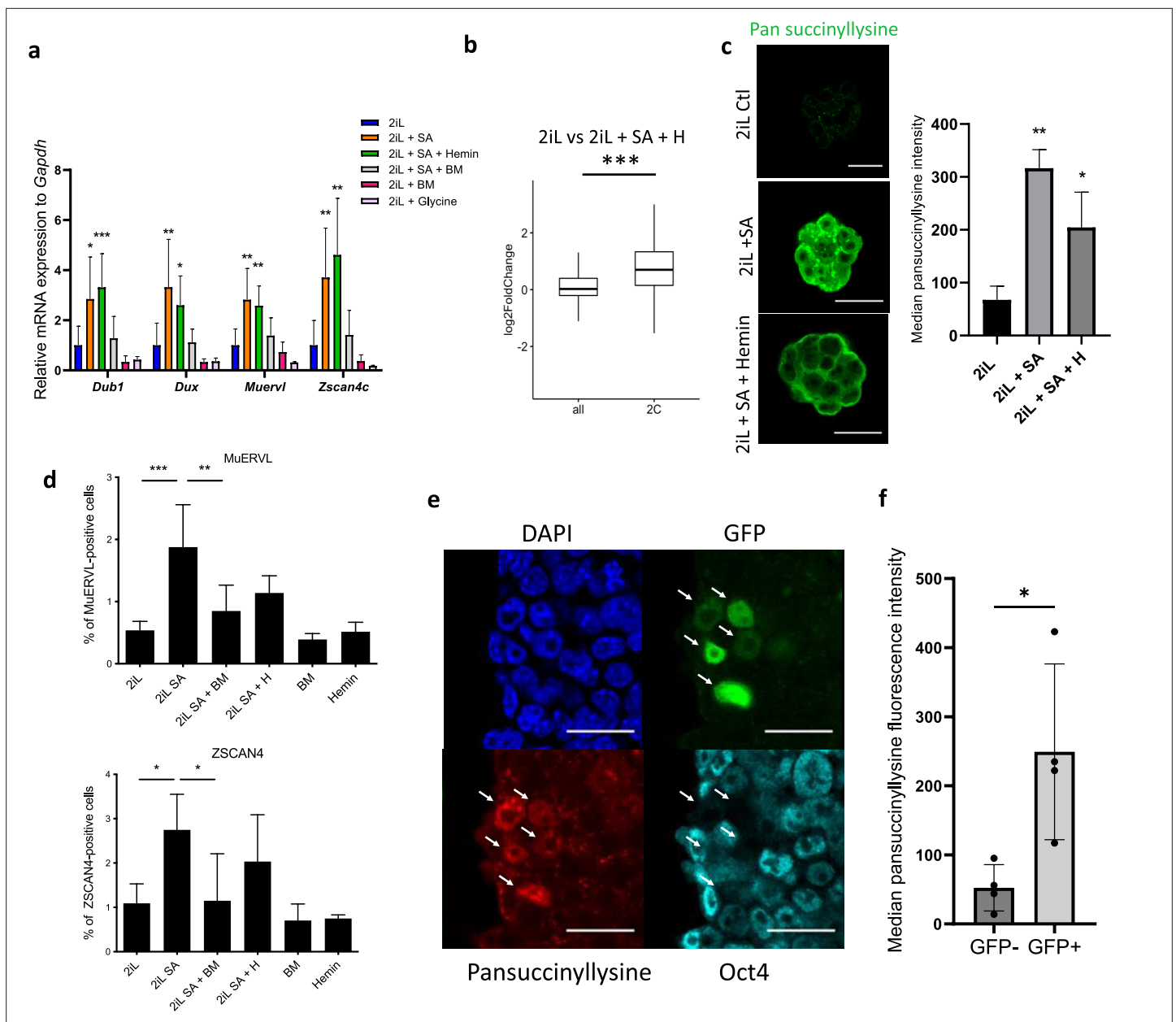
Figure 4. mESC '2C-like' reprogramming by SA is due to extramitochondrial succinate accumulation. (**a**) Relative expression of 2 C markers of mESCs assessed by RT-qPCR relative to *Gapdh* expression and normalized to 2iL naive control, in mESCs treated for 2 days with 0.5 mM SA (2iL SA), with or without 10 µM Hemin (2iL SA + H), 1 µM diethyl butylmalonate (2iL SA + BM), 1 µM BM alone (BM) or 10 mM glycine. S.D. * $p<0.05$, **$p<0.01$, ***$p<0.001$. ANOVA-1. n=3–6 independent biological replicates. (**b**) Boxplot of mean Log2FC of 2 C markers defined in *Macfarlan et al., 2012* or all analyzed mRNAs in 2iL + SA + H versus 2iL control cells. Statistical significance is calculated by Student T-test. $p<0.001$. (**c**) Immunostaining of succinylated lysine residues (green) in mESCs treated for 2 days with 0.5 mM SA, with or without 10 µM Hemin (SA + Hemin) and quantified by flow cytometry. Representative image of n=3 independent experiments. Scale bar = 20 µm. Results expressed as median fluorescence +/-S.D. * $p<0.05$, **$p<0.01$; ANOVA-1 (**d**) Percentage of MUERVL or ZSCAN4-positive cells in the whole population of naïve (2iL) mESCs or naive cells treated for 2 days with SA (2iL SA) with or without 10 µM hemin (2iL SA + H) or 1 µM diethyl butylmalonate (2iL SA + BM). n=4 independent biological replicates. Results expressed as mean +/-S.D. * $p<0.05$, **$p<0.01$, ***$p<0.001$; ANOVA-1. (**e**) Immunostaining of succinyllysine residues (Red) and Oct4 (cyan) of TBG4 cells (ES-E14TG2a mESCs with a 2C-GFP (green) reporter construct) (*Mills et al., 2018*). Representative image of n=3 independent experiments. Scale bar = 20 µm. Arrows indicate 2CLCs according to the GFP reporter. (**f**) Quantification of the median fluorescence intensity of the succinyllysine residues in the GFP +and GFP- populations of TBG4 mESCs separated by flow cytometry. n=4 independent biological replicates. * $p<0.05$, T-test.

The online version of this article includes the following figure supplement(s) for figure 4:

Figure supplement 1. Treatment with SA induces a delocalization of succinyllysine-modified proteins outside of mitochondria.
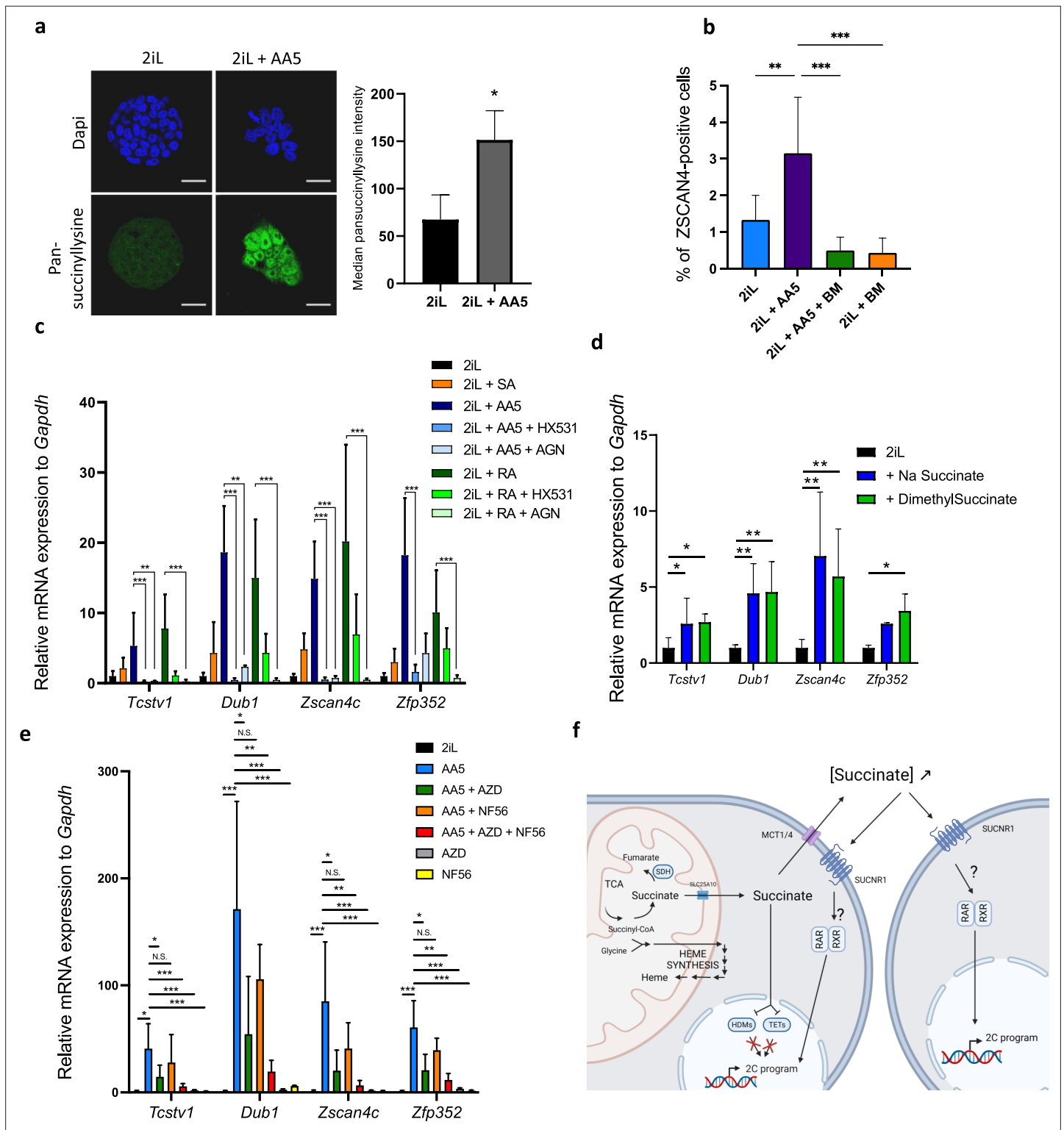
Figure 5. Inhibition of SDH leading to an increase in succinate accumulation recapitulates the increase in 2CLCs due to a leakage to the extracellular space. (**a**) Immunostaining of succinylated lysine residues (green) in mESCs in 2iL media or treated with 250 nM AA5. Representative image of n=3 independent experiments and quantified by flow cytometry. T-test. Scale bar = 20 μm (**b**) Percentage of ZSCAN4-positive cells in the whole population of naïve (2iL) mESCs or naïve treated with 250 nM AA5, with or without 1 μM diethyl butylmalonate (BM), counted from confocal micrographs with 10 images per conditions for at least 1000 cells per condition. n=3 independent biological replicates. ANOVA1 (**c**) Relative expression of the 2CLC genes in response to 250 nM AA5 or 0.5 μM retinoic acid (RA), with or without 10 μM HX531 and 100 nM AGN193109. (**d-e**) Relative expression of

Figure 5 continued on next page

Figure 5 continued

2C-gene markers of mESCs assessed by RT-qPCR relative to *Gapdh* expression in naïve 2iL mESCs and treated with 16 mM dimethyl succinate, 40 mM sodium succinate (Na succinate), 1 µM of MCT1 and 4 inhibitor (AZD3965; AZD) and 1 µM SUCNR1 receptor antagonist (NF-56-EJ40; NF56). Data shown as mean +/-S.D. *p<0.05, **p<0.01, ***p<0.001. ANOVA-1 followed by a Tukey post-test. n=4 independent biological replicates. (**f**) Graphical representation of the succinate-induced 2CLC reprogramming. Created with https://www.biorender.com/.

The online version of this article includes the following figure supplement(s) for figure 5:

Figure supplement 1. Treatment with SA or AA5 does not trigger HIF1α stabilization.

Figure supplement 2. Treatment with SA or AA5 triggers an increase of the methylation of histones and DNA that does not cause a 2C-like reprogramming.

methylcytosine dioxygenases and the histone demethylases (HDM). Of these three classes, we ruled out a role for PHDs, responsible for HIF1α degradation, as the abundance of this transcription factor was not increased by SA nor by AA5 treatment, demonstrating a lack of stabilization following a putative PHD inhibition (*Figure 5—figure supplement 1*). Since recent reports in the literature have highlighted a crucial role of the epigenetic landscape and a role of the TET proteins in the acquisition of the 2CLC phenotype (*Eckersley-Maslin et al., 2016*; *Huang et al., 2021*; *Schüle et al., 2019*; *Lu et al., 2014*; *Yang et al., 2016*), we then focused our attention on the histone 3 (H3) and DNA methylation landscapes and observed a robust increase in the amount of trimethylation of lysines 4, 9, and 27 of H3 (H3K4,-K9, -K27) along with an increase in the global abundance of 5mC when mESCs were treated with either SA or AA5 (*Figure 5—figure supplement 2a-d*). However, chemical inhibition of HDMs by JIB04 (*Wang et al., 2013*) and/or TET by TETin-C35 (*Singh et al., 2020*) does not trigger a rise in the proportion of 2CLCs or in 2 C marker expression (*Figure 5—figure supplement 2e-f*). We then suspected that succinate could act instead as a paracrine signal after its release in the extracellular media. Indeed, exogenous supplementation with a membrane impermeable (sodium succinate) or permeable (dimethylsuccinate) form of succinate were able to increase the 2CLC marker expression (*Figure 5d*). We further found that inhibition of the succinate exit through the plasma membrane, by targeting MCT1 and 4 with the AZD3965 inhibitor (*Beloueche-Babari et al., 2017*; *Reddy et al., 2020*) combined to inhibition of the succinate receptor SUCNR1 by NF-56-EJ40 (*Haffke et al., 2019*) is able to bring down the rise in 2CLC marker expression triggered by AA5 (*Figure 5e*). Recent reports have shown that retinoic acid (RA) also increases the 2CLC population, an effect mediated by the retinoic acid receptor RAR but not the RXRs (*Iturbide et al., 2021*). While the induction of the 2CLC gene signature in response to AA5 is similar to RA, the mode of action seems to involve both RAR and RXR since the effect is rescued by addition of both inhibitors, AGN193109 and HX531, respectively (*Figure 5c*). These findings strongly support succinate acting as a paracrine/autocrine signal upstream of RAR/RXR transcriptional activity. Together, these sets of data highlight the critical role of succinate in the acquisition and maintenance of pluri/totipotent states in mESCs by a totally new mechanism.

Discussion

The comparison of two different genome-scale CRISPR screens in the exit of the naïve state of mouse and human ESCs (*Mathieu et al., 2019*; *Li et al., 2018*) revealed the importance of heme biosynthesis for the transition to another pluripotent state, the primed state. Using succinyl acetone (SA), a specific inhibitor of ALAD that catalyzes the second reaction of the pathway, and hemin to rescue the heme defect, we first confirmed the requirement of this pathway for the naive-to-primed transition in mESCs. This is in accordance with the embryonic lethality at the implantation stage of mouse embryos knockout for the heme synthesis pathway enzymes since the naïve-to-primed transition recapitulates, in vitro, this critical step (shown for HMBS *Lindberg et al., 1996*, UROS *Bensidhoum, 1998*, UROD *Phillips et al., 2001*, CPOX *Conway et al., 2017* and FECH *Magness et al., 2002*). RNAseq analysis of naïve cells undergoing transition to the primed stage in the presence of SA with or without addition of hemin revealed a failure to properly activate the MAPK and TGFβ-SMAD pathways in response to heme biosynthesis inhibition. It has been previously demonstrated that the proper activation of these two pathways is required to proceed with the transition to the primed stage (*Tsanov et al., 2017*; *Jiapaer et al., 2018*; *Senft et al., 2018*; *Arman et al., 1998*). While the inhibition of SMAD3 was able to mimic the effect observed by heme synthesis inhibition, the inhibition of MAPK by MEK inhibition proved to be inefficient at blocking the process, in contradiction to its role in the

progression of pluripotency (*Tsanov et al., 2017*; *Jiapaer et al., 2018*; *Arman et al., 1998*). Such a connection between heme synthesis inhibition and signaling pathways has only been reported once in PC12 neuronal cells, with SA blocking the activation of the MAPK despite the presence of nerve growth factor (NGF) (*Zhu et al., 2002*). Thus, it seems to be a conserved mechanism among various cell identities/types, as it is also observed in our study for cells responding to FGF2 signals. While the link between heme and these crucial signaling pathways remains unknown, it brings to light a crucial importance of this metabolite and its synthesis pathway, so far poorly understood, in the context of pluripotency.

Aside from its effect on the exit of the naïve stage, we showed here that the inhibition of heme synthesis also triggers a reprogramming toward a 2C-like stage. Indeed, mESCs cultured in 2iL conditions have been previously defined as a heterogenous population that naturally includes a small percentage of cells displaying features of the two-cell stage embryo (*Macfarlan et al., 2012*; *Rodriguez-Terrones et al., 2020*). Interestingly, this 2CLC population is transient and cycles back and forth to a naive pluripotency state (*Macfarlan et al., 2012*; *Fu et al., 2020*). Unexpectedly, heme synthesis inhibition favors this reprogramming as shown by the increase in 2C-like markers in the whole population and the proportion of ZSCAN4 or MUERVL-positive cells. Strikingly, this effect is clearly dependent on the accumulation of succinate as it is (i) not rescued by hemin, (ii) blocked by inhibition of the mitochondrial succinate transporter and (iii) phenocopied by SDH inhibition. Additionally, MUERVL-positive cells spontaneously emerging in naïve ESC colonies endogenously display a high level of succinylated proteins, supporting a role for this metabolite in the identity of the 2C-like state. The role of several metabolites in the gain of 2CLC features has already been recently unveiled, highlighting a role for acetate, lactate, and D-ribose (*Rodriguez-Terrones et al., 2020*). This metabolite screening also showed a positive effect of succinate on the 2C-like features acquisition. Beyond its role in the cellular metabolism, we show here that the succinate accumulation outside mitochondria leads to a global reduction in cytosine demethylation activity of the TETs and histone demethylation as previously observed in cancers after accumulation of succinate or SDH mutations (*Letouzé et al., 2013*; *Xiao et al., 2012*). However, previous reports are somewhat discordant regarding the role of TETs in the acquisition of the 2CLC phenotype as their effect seems to be dependent on their interacting partners (*Eckersley-Maslin et al., 2016*; *Huang et al., 2021*; *Schüle et al., 2019*; *Lu et al., 2014*). For example, while TET2 could cooperate with PSPC1 (Paraspeckle Component 1) to reduce the expression of the retrotransposon *MuERVL* (*Guallar et al., 2018*), binding of the TET proteins with SMCHD1 (structural maintenance of chromosomes flexible hinge domain containing 1) prevents the demethylation of the *Dux* gene locus and thus prevents its expression (*Huang et al., 2021*). Succinate accumulation would result in a global decrease in the activity of all 3 TET isoforms, resembling those of a TET triple KO, already shown to induce the 2 C phenotype (*Lu et al., 2014*). The methylation landscape of histones, especially H3, is also highly dynamic both in vivo, at the time of the zygote genome activation (ZGA) that takes place at the 2C-stage, and in the 2CLC conversion with remodeling of H3K4me3, H3K9me3, and H3K27me3 (*Zhang et al., 2021*; *Wang et al., 2018*; *Yang et al., 2022*) (extensively reviewed in *Xia and Xie, 2020*). Similarly to the situation with the TETs, the action of HDM on the loss or acquisition of 2C-like features in vitro is complex, as loss of KDM1a (lysine demethylase 1 a) is shown to promote the expression of *Zscan4* and *MuERVL* (*Macfarlan et al., 2011*) whereas loss of KDM5a and b decreases the expression of the markers and blocks the ZGA in vivo (*Dahl et al., 2016*). However, while the literature highlights a role for these modifications of the epigenetic landscape in the 2CLC emergence, this is not supported by the data presented here. This discrepancy could be due to differences in the culture conditions, as these previous studies use mESC grown in serum +LIF conditions, while we use ground naïve mESCs (in 2iL and serum-free culture). Such difference has been previously described in the establishment of another pluripotent state of ESCs, the paused state (*Xu et al., 2022*). Interestingly, instead of an epigenetic rewiring as the major cause of 2CLC reprogramming, our data shed light on succinate acting as a paracrine/autocrine signal, able to trigger the emergence of 2CLCs by an MCT-dependent export and the activation of SUCNR1 expressing cells. Further studies are now needed to precisely dissect which downstream actors are truly responsible for the activation of the 2 C transcriptional program.

Our study thus brings an additional and different example of metabolic control of pluripotency, and adds succinate to previously reported metabolites such as S-adenosylmethionine (SAM) (*Sperber et al., 2015*), alpha-ketoglutarate (αKG) (*Carey et al., 2015*; *Tischler et al., 2019*), glutamine (*Tohyama*

et al., 2016), acetyl-CoA (*Moussaieff et al., 2015*), lactate or D-ribose (*Rodriguez-Terrones et al., 2020*) that are known to regulate the pluripotent states mostly through their contribution to modifications of the epigenetic landscape (reviewed in *Tsogtbaatar et al., 2020*). In addition to these previous studies, we highlight a role of succinate that goes beyond epigenetic landscape regulation but instead influences pluripotency regulation through protein succinylation and a paracrine effect. Further emphasis on the importance of succinate in early development is also demonstrated by the embryonic lethality of the SDH subunits in mice (*Piruat et al., 2004*; *Siebers et al., 2018*; *Lepoutre-Lussey et al., 2016*; *Takács-Vellai et al., 2021*). Altogether, these results indicate a critical role of both heme and succinate in the progression of the pluripotency continuum, ranging from the 2CLCs on one hand and to the acquisition of primed pluripotency on the other.

Materials and methods

Cell culture and ALAD ko generation

mESCs (ES-E14TG2a) or tbg4 mESCs (described in *Ishiuchi et al., 2015*) were cultured in N2B27 medium consisting of a 1:1 mixture of DMEM/F12 (Gibco, 31330–038) and Neurobasal Medium (Gibco, 21103–049) supplemented with 1 x N-2 Supplement (Gibco, 17502–048), 1 x B-27 Supplement (Gibco, 17504–044), 1/100 penicillin-streptomycin (Gibco, 15140–122), 1 x MEM nonessential amino acids (NEAA) (Gibco, 11140–035), 1 x GlutaMAX (Gibco, 35050–038), 1 x sodium-pyruvate (Gibco, 11360–039) and 0.1 mM β-mercaptoethanol (Gibco, 31350–010). Naïve mESCs were maintained on 0.2% gelatin (Sigma, G1393)-coated plates at a density of 50,000 cells/cm^2 and in N2B27 medium complemented with 10^3 U/ml of mLIF (ESGRO, ESG1107), 3 µM of GSK3 inhibitor (CHIR99021) (Peprotech, 2520691) and 1 µM of MEK inhibitor (PD0325901) (referred to as 2iL) (SelleckChem, S1036). Cells were passaged every 2–3 days using accutase (Stemcell Technologies, #07920). Cells were then collected by centrifugation at 1200 rpm for 3 min and counted before seeding. The transition to EpiSC was obtained by transferring naïve mESCs on 15 µg/ml fibronectin (Gibco, 33010–018)-coated plates at a density of 30,000 cells/cm^2 and by supplementing the N2B27 medium with 12 ng/ml of bFGF (Peprotech, 100-18B) and 20 ng/ml of activin A (Peprotech, 120–14 P). Coating proteins were incubated 1 hr before seeding. mESCs were maintained at 37 °C, 5% CO$_2$ in a humidified incubator. Human ESCs, Elf1 line, were maintained of an irradiated MEF monolayer and grown in either RSeT (Stemcell Technologies) medium or in a medium composed of DMEM/F-12 media supplemented with 20% knockout serum replacer (KSR), 0.1 mM nonessential amino acids (NEAA), 1 mM sodium pyruvate, penicillin/streptomycin (all from Invitrogen), 0.1 mM β-mercaptoethanol (Sigma-Aldrich), 1 µM GSK3 inhibitor (CHIR99021), 1 µM of MEK inhibitor (PD0325901), 10 ng/ml human LIF (Chemicon), 5 ng/ml IGF1 (Peprotech) and 10 ng/ml bFGF. Cells were transferred to matrigel-coated plates prior to analysis. Exit from the naïve state triggered by growing the cells in mTeSR1 (StemCell technologies) for 4 days.

For knock-out generation, one million E14 mESC were electroporated with Cas9 (0.6 µM, Sigma) and gRNA (3 µM, Synthego) as RNP complex using Amaxa nucleofector (Human Stem Cell kit 2) in presence of 10 µM Hemin 10 uM. Individual colonies were hand-picked and plated into 96-well plates. DNA was extracted using Quick Extract DNA extraction solution (Epicentre#QE09050) and nested PCR was performed. The PCR product was purified using EXO-SAP enzyme (Thermo Fisher) and sent for Sanger sequencing analysis (through Genewiz).

Lines were routinely tested for mycoplasma and STR authenticated.

mESC treatment

The heme inhibitor succinylacetone (SA) (Sigma, D1415) is used at a concentration of 0.5 mM. Hemin (Sigma, 51280) is used at a concentration of 10 µM in 0.1 N NaOH. Diethyl butylmalonate (BM) (Sigma, 112038) is used at a concentration of 1 mM. Atpenin A5 (Santa Cruz biotechnology, sc-202475) is used at 250 nM. SIS3 (Selleck chemicals, S7959) is used at 5 µM. NF-56-EJ40 (Axon Medchem 3056) is used at 1 µM. AZD3965 (Selleckchem S7339) is used at 1 µM. Exogenous succinate is provided as either 40 mM Sodium succinate (Sigma) or 16 mM dimethylsuccinate (Sigma) supplementation. HDM inhibition was achieved with 250 nM JIB04 (Medchem express HY-13953) and TET inhibition with 5 µM TETin-C35 (Aobious AOB11121). For retinoic acid experiments, RA, HY-14649, HX531 (HY-108521) and AGN193109 (HY-U00449) were used at 0.5 µM, 10 µM and 100 nM, respectively

(all from Medchemexpress). Inhibition of Sirt7 is achieved using 5 µM of the Sirt7 inhibitor 97491 (MedChemExpress).

RNA extraction and RT-qPCR

RNA was extracted after 2 days of culture with the ReliaPrep RNA Tissue Miniprep System (Promega, Z6111) following manufacturer's protocol for non-fibrous tissue by adding RNA lysis buffer on pelleted cells. RNA concentrations were quantified with the Nanophotometer N60 (Implen). Reverse transcription (RT) was performed with the GoScript Reverse Transcriptase kit Random Primers (Promega, A2801) to convert 1 µg of RNA into cDNA. Briefly, RNA was mixed with RNAse-free water to obtain 1 µg of RNA in 12 µL and heated 5 min at 70 °C. Then, 8 µL of RT mix (4 µL random primers buffer, 2 µL enzyme, 2 µL RNAse free water) was added and the reaction was performed in a thermocycler (5 min at 25 °C, 60 min at 20 °C and 15 min at 70 °C).

The qPCR was performed on the ViiA 7 Real-Time PCR System (Thermo Fisher) with 10 ng of cDNA per reaction, SYBR Green GoTaq qPCR Master Mix (Promega, A6002) and primers listed in the *Table 2* at a final concentration of 300 nM. Altogether, 2 µL of cDNA (5 ng/µL), 1 µL of forward primer (6 µM), 1 µL of reverse primer (6 µM), 10 µL of Master Mix and 6 µL of RNAse-free water were added in each well. Relative expression was calculated using the $2^{-\Delta Ct}$ method with GAPDH as an endogenous control.

Western blot analyses

Pellets of cells were lysed by adding protein lysis buffer 20 mM Tris-HCl; pH 7.5, 150 mM NaCl, 15% Glycerol, 2% SDS, 25 x protease inhibitor cocktail (PIC, cOmplete protease inhibitor cocktail, Roche 11697498001), 25 x phosphatase inhibitor buffer (PIB, composed of 25 mM Na_3VO_3, 250 mM 4-nitrophenylphosphate, 250 mM β-glycerophosphate and 125 mM NaF), 1% TRITON X-100, SuperNuclease (Sino Biologicals, 25 U/10 µL) and by pipetting up and down. The protein concentration was determined by Pierce protein assay (ThermoFisher, 22660). Samples were mixed with Laemmli buffer (SDS, β-mercaptoethanol, Bromophenol blue) and heated for 5 min at 95 °C before loading. An amount of 10 µg of proteins were loaded on SDS-containing 10 or 12% polyacrylamide gels. At the end of migration, proteins were transferred to PVDF membranes (IPFL00010) by liquid transfer. Membranes were then blocked in LI-COR Intercept blocking buffer PBS for 1 hr at RT and incubated overnight at 4 °C with the

Table 2. List of primers used in qPCR.

Gene	Sequences (5' → 3')
Mouse	
DNMT3A	F: CTGCTGTGGAATACCCTGTTAG R: CTTTCTACCTGCTGCCATACTC
ESRRB	F: GCACCTGGGCTCTAGTTGC R: TACAGTCCTCGTAGCTCTTGC
FGF5	F: GGGATTGTAGGAATACGAGGAGTT R: CCAGAAGAATGGACGGTTGT
FGF15	F: TGTTTCACCGCTCCTTCTTT R: TTCTCCATCCTGTCGGAATC
GAPDH	F: CATGGCCTTCCGTGTTCCT R: CCTGCTTCACCACCTTCTTG
KLF2	F: CTAAAGGCGCATCTGCGTA R: TAGTGGCGGGTAAGCTCGT
KLF4	F: CCAGCAAGTCAGCTTGTGAA R: GGGCATGTTCAAGTTGGATT
OCT4	F: CACGAGTGGAAAGCAACTCA R: AGATGGTGGTCTGGCTGAAC
OTX2	F: TATCTAAAGCAACCGCCTTACG R: AAGTCCATACCCGAAGTGGTC
REX1	F: CCCTCGACAGACTGACCCTAA R: TCGGGGCTAATCTCACTTTCAT
TFCP2L1	F: GCTGGAGAATCGGAAGCTAGG R: AAAACGACACGGATGATGCTC
ZIC2	F: CAAGGTCCGGGTGCTTACC R: ATTAAAGGGAGGCCCCGAATA
TBX3	F: CTCCATTCCAGTTTGGTCAA R: CAACAGCAGCCTGGTTACAC
OCT6	F: TTTCTCAAGTGTCCCAAGCC R: ACCACCTCCTTCTCCAGTTG
DNMT3B	F: GGCAAGGACGACGTTTTGTG R: GTTGGACACGTCCGTGTAGTGAG
DUX	F: AAAGGAAGAGCATGTGCCAGC R: GCAGTAAGCTGTCCTGGGAAC
ZFP352	F: AAGTCCCACATCTGAAGAAACAC R: GGGTATGAGGATTCACCCACA
TCSTV1	F: TGAACCCTGATGCCTGCTAAGACT R: AGATGGCTGCAAAGACACAACTGC
ZSCAN4C	F: CCGGAGAAAGCAGTGAGGTGGA R: CGAAAATGCTAACAGTTGAT
MuERV-L	F: CCCATCATGAGCTGGGTACT R: CGTGCAGATCCATCAGTAAA
DUB1	F: GCAGGCCAACCTCAAACAG R: CGCAGGGCTCTCCTAAATCTT
Human	
ZSCAN4	F: TGGAAATCAAGTGGCAAAAA R: CTGCATGTGGACGTGGAC
LEUTX	F: GCTACAATGGGGAAACTGG R: CTCTTCCATTTGGCACGCTG

Table 2 continued on next page

Table 2 continued

Gene	Sequences (5' → 3')
DUX4	F: AGGAAGAATACCGGGCTCTG R: AGTCTCTCACCGGGCCTAG
TFCP2L1	Hs01011666_m1
KLF4	F: GGGAGAAGACACTGCGTCA R: GGAAGCACTGGGGGAAGT
ESRRB	hs01584024_m1
SALL1	F: AGAGAACTCACACTGGAGAG R: CATGTGTACCTTAAGATTGCCT
ETV4	F: CGACTCTGAAGATCTCTTCC R: TCATCACTGTCTGGTACCT

primary antibodies. Membranes were washed three times for 5 min with PBS +0.1% Tween-20 (PBST) before and after 1 h-incubation with the secondary antibodies at RT. Detections were performed and quantified with Odyssey LI-COR scanner. Primary and secondary antibodies were both diluted in Licor PBST. GAPDH was used as loading control. Primary and secondary antibodies for GAPDH detection were incubated 30 min. Antibodies and dilutions used are: anti-GAPDH 1:20000(Sigma, G8795), anti-KLF4 1:200 (R&D, AF3158), anti-Oct4 1:100 (Santa Cruz, sc-5279), anti-OTX2 1:100 (R&D, AF1979), anti-pan-succinyllysines 1:300 (PTM-401), anti-TFE3 1:400 (Sigma, HPA023881), anti-ZSCAN4 1:400 (Millipore, AB4340), anti-MUERVL-GAG 1:200 (Novus, NBP2-66963), anti-ERK1/2 1:1000 (Cell Signaling 9102), anti-phosphoERK1/2 1:1000 (Cell Signaling 9101), anti-SMAD2/3 1:1000(Cell Signaling 8685), anti-SMAD3 1:1000 (Abcam ab52903).

Immunofluorescence

Cells were seeded on coated glass cover (Assistent) slips 2 days before fixation with 4% paraformaldehyde (Sigma, 30525-89-4) for 15 min. Coating was performed for 1 hr with 15 µg/ml of fibronectin or with 3.5 µg/cm^2 Cell-Tak (VWR, 734–1081) diluted in 0.1 M sodium bicarbonate. Cells were permeabilized and blocked for 30 min incubation in blocking buffer (PBS, 0.1% TRITON, 1% BSA). Immunostaining was performed by an overnight incubation of cover slips at 4 °C on 30 µL drops containing primary antibody diluted in blocking buffer. After three washes of 5 min in blocking buffer, the cells were incubated for 1 hr in the dark and at RT with 30 µL drops containing secondary antibody and DAPI (Sigma, 10 236 276 001) diluted 1:1000 in blocking buffer. Cover slips were mounted with Mowiol after three washes of 5 min in blocking buffer. Analyses were performed with a Leica TCS SP5 confocal microscope (Leica microsystems). For 5mC analysis, cells were fixed for 15 min with 4% PFA, permeabilized for 10 min with PBS-0.5% Triton X-100 and treated with 4 N HCl for 20 min to denature DNA. Cells were then washed once with distilled water a 2 hr blocking with 2% BSA and 0.5% Triton X-100. After these steps, the staining process would resume as described above, using a 5mC primary antibody (Sigma SAB2702243) diluted 1:300 in blocking buffer (PBS, 0.1% TRITON, 1% BSA).

Flow cytometry

Cells were detached by a 5 min incubation with Accutase and spun for 5 min at 400 *g*. The cell pellet was then washed with PBS-10 % FBS followed by another centrifugation. The pellet, containing at least 10^6 cells, was fixed by adding 100 µl of 4% PFA for 15 min. After centrifugation, the cells were permeabilized with the Invitrogen permeabilization buffer (00833356) for 30 min at room temperature. Antibodies were incubated for 1h30 at room temperature in PBS-10 % FBS and briefly vortexed every 30 min. After three washes with PBS-10 % FBS, the cells were incubated with an anti-rabbit Alexa 647 1:1000 for 1 hr. Cell pellets were washed twice before being resuspended in PBS-10 % FBS and analysed with the FACSVerse machine. TBG4 ESCs (previously published *Eckersley-Maslin et al., 2016*) were used for pan-succinyllysine levels measure in 2CLCs, by gating the turboGFP +population and measuring the alexa 647 intensity.

RNA sequencing

Sequence libraries were prepared with the Lexogen QuantSeq 3' mRNA-Seq library prep kit according to the manufacturer's protocol. Samples were indexed to allow for multiplexing. Library quality and size range were assessed using a Bioanalyzer (Agilent Technologies) with the DNA 1000 kit (Agilent

Technologies, California, USA). Libraries were subsequently sequenced on an Illumina HiSeq4000 instrument. Single-end reads of 50 bp length were produced with a minimum of 1 M reads per sample.

Quality control of raw reads was performed with FastQC v0.11.7, available online at: http://www.bioinformatics.babraham.ac.uk/projects/fastqc. Adapters were filtered with ea-utils fastq-mcf v1.05 (Erik Aronesty (2011), ea-utils: "Command-line tools for processing biological sequencing data; https://github.com/ExpressionAnalysis/ea-utils copy archived at *Expression Analysis, 2021*). Splice-aware alignment was performed with HiSAT2 against the mouse reference genome mm10. Reads mapping to multiple loci in the reference genome were discarded. Resulting BAM files were handled with Samtools v1.5 (*Li et al., 2009*). Quantification of reads per gene was performed with HT-seq Count v2.7.14. Count-based differential expression analysis was done with R-based Bioconductor package DESeq2. Reported p-values were adjusted for multiple testing with the Benjamini-Hochberg procedure, which controls false discovery rate (FDR).

Data analysis

TMM normalized rLog transformed counts were used for Principal Component analysis using R package PCATools. Gene set enrichment analysis (GSEA) was made on gene list ranked on Log2FC using R package ClusterProfiler (*Yu et al., 2012*). For genes with FC >2 in MUERVL::Tomato$^+$ list from *Macfarlan et al., 2012*, Z score was calculated from TMM-rLog transformed counts and plotted as heatmap using R package Heatmap.plus. Analysis was made using statistical programming language R.

Statistical analysis

One-way ANOVA statistical test followed Turkey multiple comparison test or student T-Tests were conducted on all results when indicated using GraphPad Prism version 9.1.1, GraphPad Software, San Diego, California USA, https://www.graphpad.com.

Additional information

Author contributions

Damien Detraux, Conceptualization, Data curation, Formal analysis, Funding acquisition, Validation, Investigation, Visualization, Methodology, Writing – original draft, Writing – review and editing; Marino Caruso, Software, Investigation, Visualization, Methodology, Writing – review and editing; Louise Feller, Investigation, Methodology, Writing – review and editing; Maude Fransolet, Investigation;

Sébastien Meurant, Investigation, Writing – review and editing; Julie Mathieu, Conceptualization, Supervision, Writing – review and editing; Thierry Arnould, Supervision, Writing – review and editing; Patricia Renard, Conceptualization, Supervision, Writing – original draft, Writing – review and editing

Author ORCIDs
Damien Detraux [ORCID] http://orcid.org/0000-0002-9704-2076
Sébastien Meurant [ORCID] http://orcid.org/0000-0003-0711-9605
Patricia Renard [ORCID] http://orcid.org/0000-0003-4144-3353

Decision letter and Author response
Decision letter https://doi.org/10.7554/eLife.78546.sa1
Author response https://doi.org/10.7554/eLife.78546.sa2

Additional files

Supplementary files
• MDAR checklist

Data availability
Sequencing data have been deposited in GEO under the accession GSE178089. Data files for the western blot images have been added as raw images of scans.

The following dataset was generated:

Author(s)	Year	Dataset title	Dataset URL	Database and Identifier
Detraux D, Caruso M	2021	The critical role of heme synthesis in the regulation of pluripotent states is succinate-dependent	https://www.ncbi.nlm.nih.gov/geo/query/acc.cgi?acc=GSE178089	NCBI Gene Expression Omnibus, GSE178089

References

Arman E, Haffner-Krausz R, Chen Y, Heath JK, Lonai P. 1998. Targeted disruption of fibroblast growth factor (FGF) receptor 2 suggests a role for FGF signaling in pregastrulation mammalian development. *PNAS* **95**:5082–5087. DOI: https://doi.org/10.1073/pnas.95.9.5082, PMID: 9560232

Atamna H. 2004. Heme, iron, and the mitochondrial decay of ageing. *Ageing Research Reviews* **3**:303–318. DOI: https://doi.org/10.1016/j.arr.2004.02.002, PMID: 15231238

Beloueche-Babari M, Wantuch S, Casals Galobart T, Koniordou M, Parkes HG, Arunan V, Chung YL, Eykyn TR, Smith PD, Leach MO. 2017. MCT1 Inhibitor AZD3965 Increases Mitochondrial Metabolism, Facilitating Combination Therapy and Noninvasive Magnetic Resonance Spectroscopy. *Cancer Research* **77**:5913–5924. DOI: https://doi.org/10.1158/0008-5472.CAN-16-2686, PMID: 28923861

Bensidhoum M. 1998. The disruption of mouse uroporphyrinogen III synthase (uros) gene is fully lethal. *Transgenics* **2**:275–280.

Betschinger J, Nichols J, Dietmann S, Corrin PD, Paddison PJ, Smith A. 2013. Exit from pluripotency is gated by intracellular redistribution of the bHLH transcription factor Tfe3. *Cell* **153**:335–347. DOI: https://doi.org/10.1016/j.cell.2013.03.012, PMID: 23582324

Carey BW, Finley LWS, Cross JR, Allis CD, Thompson CB. 2015. Intracellular α-ketoglutarate maintains the pluripotency of embryonic stem cells. *Nature* **518**:413–416. DOI: https://doi.org/10.1038/nature13981, PMID: 25487152

Chen T, Ozel D, Qiao Y, Harbinski F, Chen L, Denoyelle S, He X, Zvereva N, Supko JG, Chorev M, Halperin JA, Aktas BH. 2011. Chemical genetics identify eIF2α kinase heme-regulated inhibitor as an anticancer target. *Nature Chemical Biology* **7**:610–616. DOI: https://doi.org/10.1038/nchembio.613, PMID: 21765405

Conway AJ, Brown FC, Fullinfaw RO, Kile BT, Jane SM, Curtis DJ. 2017. A mouse model of hereditary coproporphyria identified in an ENU mutagenesis screen. *Disease Models & Mechanisms* **10**:1005–1013. DOI: https://doi.org/10.1242/dmm.029116, PMID: 28600349

Dahl JA, Jung I, Aanes H, Greggains GD, Manaf A, Lerdrup M, Li G, Kuan S, Li B, Lee AY, Preissl S, Jermstad I, Haugen MH, Suganthan R, Bjørås M, Hansen K, Dalen KT, Fedorcsak P, Ren B, Klungland A. 2016. Broad histone H3K4me3 domains in mouse oocytes modulate maternal-to-zygotic transition. *Nature* **537**:548–552. DOI: https://doi.org/10.1038/nature19360, PMID: 27626377

Duggal G, Warrier S, Ghimire S, Broekaert D, Van der Jeught M, Lierman S, Deroo T, Peelman L, Van Soom A, Cornelissen R, Menten B, Mestdagh P, Vandesompele J, Roost M, Slieker RC, Heijmans BT, Deforce D, De Sutter P, De Sousa Lopes SC, Heindryckx B. 2015. Alternative Routes to Induce Naïve Pluripotency in

Human Embryonic Stem Cells. *Stem Cells* **33**:2686–2698. DOI: https://doi.org/10.1002/stem.2071, PMID: 26108678

Eckersley-Maslin MA, Svensson V, Krueger C, Stubbs TM, Giehr P, Krueger F, Miragaia RJ, Kyriakopoulos C, Berrens RV, Milagre I, Walter J, Teichmann SA, Reik W. 2016. MERVL/Zscan4 Network Activation Results in Transient Genome-wide DNA Demethylation of mESCs. *Cell Reports* **17**:179–192. DOI: https://doi.org/10.1016/j.celrep.2016.08.087, PMID: 27681430

Evans MJ, Kaufman MH. 1981. Establishment in culture of pluripotential cells from mouse embryos. *Nature* **292**:154–156. DOI: https://doi.org/10.1038/292154a0, PMID: 7242681

Expression Analysis. 2021. Ea-Utils. swh:1:rev:10c21926a4dce4289d5052acfd73b8e744d4fede. Software Heritage. https://archive.softwareheritage.org/swh:1:dir:57f11b13a1033a830d3b09182e3d9c3a44af4dad; origin=https://github.com/ExpressionAnalysis/ea-utils;visit=swh:1:snp:193c4deb7070aba2ebfa36e2d8e6461e b6fd3ecb;anchor=swh:1:rev:10c21926a4dce4289d5052acfd73b8e744d4fede

Fu X, Djekidel MN, Zhang Y. 2020. A transcriptional roadmap for 2C-like-to-pluripotent state transition. *Science Advances* **6**:eaay5181. DOI: https://doi.org/10.1126/sciadv.aay5181, PMID: 32523982

Gafni O, Weinberger L, Mansour AA, Manor YS, Chomsky E, Ben-Yosef D, Kalma Y, Viukov S, Maza I, Zviran A, Rais Y, Shipony Z, Mukamel Z, Krupalnik V, Zerbib M, Geula S, Caspi I, Schneir D, Shwartz T, Gilad S, et al. 2013. Derivation of novel human ground state naive pluripotent stem cells. *Nature* **504**:282–286. DOI: https://doi.org/10.1038/nature12745, PMID: 24172903

Grow EJ, Flynn RA, Chavez SL, Bayless NL, Wossidlo M, Wesche DJ, Martin L, Ware CB, Blish CA, Chang HY, Pera RAR, Wysocka J. 2015. Intrinsic retroviral reactivation in human preimplantation embryos and pluripotent cells. *Nature* **522**:221–225. DOI: https://doi.org/10.1038/nature14308, PMID: 25896322

Guallar D, Bi X, Pardavila JA, Huang X, Saenz C, Shi X, Zhou H, Faiola F, Ding J, Haruehanroengra P, Yang F, Li D, Sanchez-Priego C, Saunders A, Pan F, Valdes VJ, Kelley K, Blanco MG, Chen L, Wang H, et al. 2018. RNA-dependent chromatin targeting of TET2 for endogenous retrovirus control in pluripotent stem cells. *Nature Genetics* **50**:443–451. DOI: https://doi.org/10.1038/s41588-018-0060-9, PMID: 29483655

Haffke M, Fehlmann D, Rummel G, Boivineau J, Duckely M, Gommermann N, Cotesta S, Sirockin F, Freuler F, Littlewood-Evans A, Kaupmann K, Jaakola VP. 2019. Structural basis of species-selective antagonist binding to the succinate receptor. *Nature* **574**:581–585. DOI: https://doi.org/10.1038/s41586-019-1663-8, PMID: 31645725

Huang Z, Yu J, Cui W, Johnson BK, Kim K, Pfeifer GP. 2021. The chromosomal protein SMCHD1 regulates DNA methylation and the 2c-like state of embryonic stem cells by antagonizing TET proteins. *Science Advances* **7**:eabb9149. DOI: https://doi.org/10.1126/sciadv.abb9149, PMID: 33523915

Ishiuchi T, Enriquez-Gasca R, Mizutani E, Bošković A, Ziegler-Birling C, Rodriguez-Terrones D, Wakayama T, Vaquerizas JM, Torres-Padilla ME. 2015. Early embryonic-like cells are induced by downregulating replication-dependent chromatin assembly. *Nature Structural & Molecular Biology* **22**:662–671. DOI: https://doi.org/10.1038/nsmb.3066, PMID: 26237512

Iturbide A, Ruiz Tejada Segura ML, Noll C, Schorpp K, Rothenaigner I, Ruiz-Morales ER, Lubatti G, Agami A, Hadian K, Scialdone A, Torres-Padilla M-E. 2021. Retinoic acid signaling is critical during the totipotency window in early mammalian development. *Nature Structural & Molecular Biology* **28**:521–532. DOI: https://doi.org/10.1038/s41594-021-00590-w, PMID: 34045724

Jiapaer Z, Li G, Ye D, Bai M, Li J, Guo X, Du Y, Su D, Jia W, Chen W, Wang G, Yu Y, Zhu F, Wan X, Kang J. 2018. LincU Preserves Naïve Pluripotency by Restricting ERK Activity in Embryonic Stem Cells. *Stem Cell Reports* **11**:395–409. DOI: https://doi.org/10.1016/j.stemcr.2018.06.010, PMID: 30017820

Kim HJ, Khalimonchuk O, Smith PM, Winge DR. 2012. Structure, function, and assembly of heme centers in mitochondrial respiratory complexes. *Biochimica et Biophysica Acta* **1823**:1604–1616. DOI: https://doi.org/10.1016/j.bbamcr.2012.04.008, PMID: 22554985

Lämsä V, Levonen AL, Sormunen R, Yamamoto M, Hakkola J. 2012. Heme and heme biosynthesis intermediates induce heme oxygenase-1 and cytochrome P450 2A5, enzymes with putative sequential roles in heme and bilirubin metabolism: different requirement for transcription factor nuclear factor erythroid- derived 2-like 2. *Toxicological Sciences* **130**:132–144. DOI: https://doi.org/10.1093/toxsci/kfs237, PMID: 22859313

Lepoutre-Lussey C, Thibault C, Buffet A, Morin A, Badoual C, Bénit P, Rustin P, Ottolenghi C, Janin M, Castro-Vega LJ, Trapman J, Gimenez-Roqueplo AP, Favier J. 2016. From Nf1 to Sdhb knockout: Successes and failures in the quest for animal models of pheochromocytoma. *Molecular and Cellular Endocrinology* **421**:40–48. DOI: https://doi.org/10.1016/j.mce.2015.06.027, PMID: 26123588

Letouzé E, Martinelli C, Loriot C, Burnichon N, Abermil N, Ottolenghi C, Janin M, Menara M, Nguyen AT, Benit P, Buffet A, Marcaillou C, Bertherat J, Amar L, Rustin P, De Reyniès A, Gimenez-Roqueplo A-P, Favier J. 2013. SDH mutations establish a hypermethylator phenotype in paraganglioma. *Cancer Cell* **23**:739–752. DOI: https://doi.org/10.1016/j.ccr.2013.04.018, PMID: 23707781

Li H, Handsaker B, Wysoker A, Fennell T, Ruan J, Homer N, Marth G, Abecasis G, Durbin R, 1000 Genome Project Data Processing Subgroup. 2009. The Sequence Alignment/Map format and SAMtools. *Bioinformatics* **25**:2078–2079. DOI: https://doi.org/10.1093/bioinformatics/btp352, PMID: 19505943

Li M, Yu JSL, Tilgner K, Ong SH, Koike-Yusa H, Yusa K. 2018. Genome-wide CRISPR-KO Screen Uncovers mTORC1-Mediated Gsk3 Regulation in Naive Pluripotency Maintenance and Dissolution. *Cell Reports* **24**:489–502. DOI: https://doi.org/10.1016/j.celrep.2018.06.027, PMID: 29996108

Li QV, Rosen BP, Huangfu D. 2020. Decoding pluripotency: Genetic screens to interrogate the acquisition, maintenance, and exit of pluripotency. *Wiley Interdisciplinary Reviews. Systems Biology and Medicine* **12**:e1464. DOI: https://doi.org/10.1002/wsbm.1464, PMID: 31407519

Lindberg RLP, Porcher C, Grandchamp B, Ledermann B, Bürki K, Brandner S, Aguzzi A, Meyer UA. 1996. Porphobilinogen deaminase deficiency in mice causes a neuropathy resembling that of human hepatic porphyria. *Nature Genetics* **12**:195–199. DOI: https://doi.org/10.1038/ng0296-195, PMID: 8563760

Lu F, Liu Y, Jiang L, Yamaguchi S, Zhang Y. 2014. Role of Tet proteins in enhancer activity and telomere elongation. *Genes & Development* **28**:2103–2119. DOI: https://doi.org/10.1101/gad.248005.114, PMID: 25223896

Macfarlan TS, Gifford WD, Agarwal S, Driscoll S, Lettieri K, Wang J, Andrews SE, Franco L, Rosenfeld MG, Ren B, Pfaff SL. 2011. Endogenous retroviruses and neighboring genes are coordinately repressed by LSD1/KDM1A. *Genes & Development* **25**:594–607. DOI: https://doi.org/10.1101/gad.2008511, PMID: 21357675

Macfarlan TS, Gifford WD, Driscoll S, Lettieri K, Rowe HM, Bonanomi D, Firth A, Singer O, Trono D, Pfaff SL. 2012. Embryonic stem cell potency fluctuates with endogenous retrovirus activity. *Nature* **487**:57–63. DOI: https://doi.org/10.1038/nature11244, PMID: 22722858

Magness ST, Maeda N, Brenner DA. 2002. An exon 10 deletion in the mouse ferrochelatase gene has a dominant-negative effect and causes mild protoporphyria. *Blood* **100**:1470–1477. DOI: https://doi.org/10.1182/blood-2001-12-0283, PMID: 12149233

Martin GR. 1981. Isolation of a pluripotent cell line from early mouse embryos cultured in medium conditioned by teratocarcinoma stem cells. *PNAS* **78**:7634–7638. DOI: https://doi.org/10.1073/pnas.78.12.7634, PMID: 6950406

Mathieu J, Detraux D, Kuppers D, Wang Y, Cavanaugh C, Sidhu S, Levy S, Robitaille AM, Ferreccio A, Bottorff T, McAlister A, Somasundaram L, Artoni F, Battle S, Hawkins RD, Moon RT, Ware CB, Paddison PJ, Ruohola-Baker H. 2019. Folliculin regulates mTORC1/2 and WNT pathways in early human pluripotency. *Nature Communications* **10**:632. DOI: https://doi.org/10.1038/s41467-018-08020-0, PMID: 30733432

Mills EL, Pierce KA, Jedrychowski MP, Garrity R, Winther S, Vidoni S, Yoneshiro T, Spinelli JB, Lu GZ, Kazak L, Banks AS, Haigis MC, Kajimura S, Murphy MP, Gygi SP, Clish CB, Chouchani ET. 2018. Accumulation of succinate controls activation of adipose tissue thermogenesis. *Nature* **560**:102–106. DOI: https://doi.org/10.1038/s41586-018-0353-2, PMID: 30022159

Miyadera H, Shiomi K, Ui H, Yamaguchi Y, Masuma R, Tomoda H, Miyoshi H, Osanai A, Kita K, Omura S. 2003. Atpenins, potent and specific inhibitors of mitochondrial complex II (succinate-ubiquinone oxidoreductase). *PNAS* **100**:473–477. DOI: https://doi.org/10.1073/pnas.0237315100, PMID: 12515859

Moussaieff A, Rouleau M, Kitsberg D, Cohen M, Levy G, Barasch D, Nemirovski A, Shen-Orr S, Laevsky I, Amit M, Bomze D, Elena-Herrmann B, Scherf T, Nissim-Rafinia M, Kempa S, Itskovitz-Eldor J, Meshorer E, Aberdam D, Nahmias Y. 2015. Glycolysis-mediated changes in acetyl-CoA and histone acetylation control the early differentiation of embryonic stem cells. *Cell Metabolism* **21**:392–402. DOI: https://doi.org/10.1016/j.cmet.2015.02.002, PMID: 25738455

Nichols J, Smith A. 2009. Naive and primed pluripotent states. *Cell Stem Cell* **4**:487–492. DOI: https://doi.org/10.1016/j.stem.2009.05.015, PMID: 19497275

Pakos-Zebrucka K, Koryga I, Mnich K, Ljujic M, Samali A, Gorman AM. 2016. The integrated stress response. *EMBO Reports* **17**:1374–1395. DOI: https://doi.org/10.15252/embr.201642195, PMID: 27629041

Percharde M, Lin CJ, Yin Y, Guan J, Peixoto GA, Bulut-Karslioglu A, Biechele S, Huang B, Shen X, Ramalho-Santos M. 2018. A LINE1-Nucleolin Partnership Regulates Early Development and ESC Identity. *Cell* **174**:391–405. DOI: https://doi.org/10.1016/j.cell.2018.05.043, PMID: 29937225

Phillips JD, Jackson LK, Bunting M, Franklin MR, Thomas KR, Levy JE, Andrews NC, Kushner JP. 2001. A mouse model of familial porphyria cutanea tarda. *PNAS* **98**:259–264. DOI: https://doi.org/10.1073/pnas.98.1.259, PMID: 11134514

Piruat JI, Pintado CO, Ortega-Sáenz P, Roche M, López-Barneo J. 2004. The mitochondrial SDHD gene is required for early embryogenesis, and its partial deficiency results in persistent carotid body glomus cell activation with full responsiveness to hypoxia. *Molecular and Cellular Biology* **24**:10933–10940. DOI: https://doi.org/10.1128/MCB.24.24.10933-10940.2004, PMID: 15572694

Reddy A, Bozi LHM, Yaghi OK, Mills EL, Xiao H, Nicholson HE, Paschini M, Paulo JA, Garrity R, Laznik-Bogoslavski D, Ferreira JCB, Carl CS, Sjøberg KA, Wojtaszewski JFP, Jeppesen JF, Kiens B, Gygi SP, Richter EA, Mathis D, Chouchani ET. 2020. pH-Gated Succinate Secretion Regulates Muscle Remodeling in Response to Exercise. *Cell* **183**:62–75. DOI: https://doi.org/10.1016/j.cell.2020.08.039, PMID: 32946811

Rodriguez-Terrones D, Hartleben G, Gaume X, Eid A, Guthmann M, Iturbide A, Torres-Padilla ME. 2020. A distinct metabolic state arises during the emergence of 2-cell-like cells. *EMBO Reports* **21**:e48354. DOI: https://doi.org/10.15252/embr.201948354, PMID: 31849178

Sahakyan A, Kim R, Chronis C, Sabri S, Bonora G, Theunissen TW, Kuoy E, Langerman J, Clark AT, Jaenisch R, Plath K. 2017. Human Naive Pluripotent Stem Cells Model X Chromosome Dampening and X Inactivation. *Cell Stem Cell* **20**:87–101. DOI: https://doi.org/10.1016/j.stem.2016.10.006, PMID: 27989770

Sassa S, Kappas A. 1983. Hereditary tyrosinemia and the heme biosynthetic pathway profound inhibition of delta-aminolevulinic acid dehydratase activity by succinylacetone. *The Journal of Clinical Investigation* **71**:625–634. DOI: https://doi.org/10.1172/jci110809, PMID: 6826727

Schüle KM, Leichsenring M, Andreani T, Vastolo V, Mallick M, Musheev MU, Karaulanov E, Niehrs C. 2019. GADD45 promotes locus-specific DNA demethylation and 2C cycling in embryonic stem cells. *Genes & Development* **33**:782–798. DOI: https://doi.org/10.1101/gad.325696.119, PMID: 31171699

Senft AD, Costello I, King HW, Mould AW, Bikoff EK, Robertson EJ. 2018. Combinatorial Smad2/3 Activities Downstream of Nodal Signaling Maintain Embryonic/Extra-Embryonic Cell Identities during Lineage Priming. *Cell Reports* **24**:1977–1985. DOI: https://doi.org/10.1016/j.celrep.2018.07.077, PMID: 30134160

Siebers EM, Choi MJ, Tinklenberg JA, Beatka MJ, Ayres S, Meng H, Helbling DC, Takizawa A, Bennett B, Garces AM, Dias Duarte Machado LG, Dimmock D, Dwinell MR, Geurts AM, Lawlor MW. 2018. Sdha+/- Rats Display Minimal Muscle Pathology Without Significant Behavioral or Biochemical Abnormalities. *Journal of Neuropathology and Experimental Neurology* **77**:665–672. DOI: https://doi.org/10.1093/jnen/nly042, PMID: 29850869

Singh AK, Zhao B, Liu X, Wang X, Li H, Qin H, Wu X, Ma Y, Horne D, Yu X. 2020. Selective targeting of TET catalytic domain promotes somatic cell reprogramming. *PNAS* **117**:3621–3626. DOI: https://doi.org/10.1073/pnas.1910702117, PMID: 32024762

Smestad J, Erber L, Chen Y, Maher LJ. 2018. Chromatin Succinylation Correlates with Active Gene Expression and Is Perturbed by Defective TCA Cycle Metabolism. *iScience* **2**:63–75. DOI: https://doi.org/10.1016/j.isci.2018.03.012, PMID: 29888767

Sperber H, Mathieu J, Wang Y, Ferreccio A, Hesson J, Xu Z, Fischer KA, Devi A, Detraux D, Gu H, Battle SL, Showalter M, Valensisi C, Bielas JH, Ericson NG, Margaretha L, Robitaille AM, Margineantu D, Fiehn O, Hockenbery D, et al. 2015. The metabolome regulates the epigenetic landscape during naive-to-primed human embryonic stem cell transition. *Nature Cell Biology* **17**:1523–1535. DOI: https://doi.org/10.1038/ncb3264, PMID: 26571212

Sustáčková G, Legartová S, Kozubek S, Stixová L, Pacherník J, Bártová E. 2012. Differentiation-independent fluctuation of pluripotency-related transcription factors and other epigenetic markers in embryonic stem cell colonies. *Stem Cells and Development* **21**:710–720. DOI: https://doi.org/10.1089/scd.2011.0085, PMID: 21609209

Taelman J, Popovic M, Bialecka M, Tilleman L, Warrier S, Van Der Jeught M, Menten B, Deforce D, De Sutter P, Van Nieuwerburgh F, Abe K, Heindryckx B, Chuva de Sousa Lopes SM. 2019. WNT Inhibition and Increased FGF Signaling Promotes Derivation of Less Heterogeneous Primed Human Embryonic Stem Cells, Compatible with Differentiation. *Stem Cells and Development* **28**:579–592. DOI: https://doi.org/10.1089/scd.2018.0199, PMID: 30827199

Takács-Vellai K, Farkas Z, Ősz F, Stewart GW. 2021. Model systems in SDHx-related pheochromocytoma/paraganglioma. *Cancer Metastasis Reviews* **40**:1177–1201. DOI: https://doi.org/10.1007/s10555-021-10009-z, PMID: 34957538

Takashima Y, Guo G, Loos R, Nichols J, Ficz G, Krueger F, Oxley D, Santos F, Clarke J, Mansfield W, Reik W, Bertone P, Smith A. 2014. Resetting transcription factor control circuitry toward ground-state pluripotency in human. *Cell* **158**:1254–1269. DOI: https://doi.org/10.1016/j.cell.2014.08.029, PMID: 25215486

Taubenschmid-Stowers J, Rostovskaya M, Santos F, Ljung S, Argelaguet R, Krueger F, Nichols J, Reik W. 2022. 8C-like cells capture the human zygotic genome activation program in vitro. *Cell Stem Cell* **29**:449–459. DOI: https://doi.org/10.1016/j.stem.2022.01.014, PMID: 35216671

Theunissen TW, Friedli M, He Y, Planet E, O'Neil RC, Markoulaki S, Pontis J, Wang H, Iouranova A, Imbeault M, Duc J, Cohen MA, Wert KJ, Castanon R, Zhang Z, Huang Y, Nery JR, Drotar J, Lungjangwa T, Trono D, et al. 2016. Molecular Criteria for Defining the Naive Human Pluripotent State. *Cell Stem Cell* **19**:502–515. DOI: https://doi.org/10.1016/j.stem.2016.06.011, PMID: 27424783

Thomson JA, Itskovitz-Eldor J, Shapiro SS, Waknitz MA, Swiergiel JJ, Marshall VS, Jones JM. 1998. Embryonic stem cell lines derived from human blastocysts. *Science* **282**:1145–1147. DOI: https://doi.org/10.1126/science.282.5391.1145, PMID: 9804556

Tischler J, Gruhn WH, Reid J, Allgeyer E, Buettner F, Marr C, Theis F, Simons BD, Wernisch L, Surani MA. 2019. Metabolic regulation of pluripotency and germ cell fate through α-ketoglutarate. *The EMBO Journal* **38**:e99518. DOI: https://doi.org/10.15252/embj.201899518, PMID: 30257965

Tohyama S, Fujita J, Hishiki T, Matsuura T, Hattori F, Ohno R, Kanazawa H, Seki T, Nakajima K, Kishino Y, Okada M, Hirano A, Kuroda T, Yasuda S, Sato Y, Yuasa S, Sano M, Suematsu M, Fukuda K. 2016. Glutamine Oxidation Is Indispensable for Survival of Human Pluripotent Stem Cells. *Cell Metabolism* **23**:663–674. DOI: https://doi.org/10.1016/j.cmet.2016.03.001, PMID: 27050306

Tsanov KM, Pearson DS, Wu Z, Han A, Triboulet R, Seligson MT, Powers JT, Osborne JK, Kane S, Gygi SP, Gregory RI, Daley GQ. 2017. LIN28 phosphorylation by MAPK/ERK couples signalling to the post-transcriptional control of pluripotency. *Nature Cell Biology* **19**:60–67. DOI: https://doi.org/10.1038/ncb3453, PMID: 27992407

Tsogtbaatar E, Landin C, Minter-Dykhouse K, Folmes CDL. 2020. Energy Metabolism Regulates Stem Cell Pluripotency. *Frontiers in Cell and Developmental Biology* **8**:87. DOI: https://doi.org/10.3389/fcell.2020.00087, PMID: 32181250

Vinchi F, Ingoglia G, Chiabrando D, Mercurio S, Turco E, Silengo L, Altruda F, Tolosano E. 2014. Heme exporter FLVCR1a regulates heme synthesis and degradation and controls activity of cytochromes P450. *Gastroenterology* **146**:1325–1338. DOI: https://doi.org/10.1053/j.gastro.2014.01.053, PMID: 24486949

Wang L, Chang J, Varghese D, Dellinger M, Kumar S, Best AM, Ruiz J, Bruick R, Peña-Llopis S, Xu J, Babinski DJ, Frantz DE, Brekken RA, Quinn AM, Simeonov A, Easmon J, Martinez ED. 2013. A small molecule modulates Jumonji histone demethylase activity and selectively inhibits cancer growth. *Nature Communications* **4**:1–13. DOI: https://doi.org/10.1038/ncomms3035, PMID: 23792809

Wang C, Liu X, Gao Y, Yang L, Li C, Liu W, Chen C, Kou X, Zhao Y, Chen J, Wang Y, Le R, Wang H, Duan T, Zhang Y, Gao S. 2018. Reprogramming of H3K9me3-dependent heterochromatin during mammalian embryo development. *Nature Cell Biology* **20**:620–631. DOI: https://doi.org/10.1038/s41556-018-0093-4, PMID: 29686265

Ware CB, Nelson AM, Mecham B, Hesson J, Zhou W, Jonlin EC, Jimenez-Caliani AJ, Deng X, Cavanaugh C, Cook S, Tesar PJ, Okada J, Margaretha L, Sperber H, Choi M, Blau CA, Treuting PM, Hawkins RD, Cirulli V, Ruohola-Baker H. 2014. Derivation of naive human embryonic stem cells. *PNAS* **111**:4484–4489. DOI: https://doi.org/10.1073/pnas.1319738111, PMID: 24623855

Xia W, Xie W. 2020. Rebooting the Epigenomes during Mammalian Early Embryogenesis. *Stem Cell Reports* **15**:1158–1175. DOI: https://doi.org/10.1016/j.stemcr.2020.09.005, PMID: 33035464

Xiao M, Yang H, Xu W, Ma S, Lin H, Zhu H, Liu L, Liu Y, Yang C, Xu Y, Zhao S, Ye D, Xiong Y, Guan K-L. 2012. Inhibition of α-KG-dependent histone and DNA demethylases by fumarate and succinate that are accumulated in mutations of FH and SDH tumor suppressors. *Genes & Development* **26**:1326–1338. DOI: https://doi.org/10.1101/gad.191056.112, PMID: 22677546

Xu Z, Robitaille AM, Berndt JD, Davidson KC, Fischer KA, Mathieu J, Potter JC, Ruohola-Baker H, Moon RT. 2016. Wnt/β-catenin signaling promotes self-renewal and inhibits the primed state transition in naïve human embryonic stem cells. *PNAS* **113**:E6382–E6390. DOI: https://doi.org/10.1073/pnas.1613849113, PMID: 27698112

Xu X, Ahmed T, Wang L, Cao X, Zhang Z, Wang M, Lv Y, Kanwal S, Tariq M, Lin R, Zhang H, Huang Y, Peng H, Lin D, Shi X, Geng D, Liu B, Zhang X, Yi W, Qin Y, et al. 2022. The mTORC1-eIF4F axis controls paused pluripotency. *EMBO Reports* **23**:e53081. DOI: https://doi.org/10.15252/embr.202153081, PMID: 34866316

Yang J, Guo R, Wang H, Ye X, Zhou Z, Dan J, Wang H, Gong P, Deng W, Yin Y, Mao S, Wang L, Ding J, Li J, Keefe DL, Dawlaty MM, Wang J, Xu G, Liu L. 2016. Tet Enzymes Regulate Telomere Maintenance and Chromosomal Stability of Mouse ESCs. *Cell Reports* **15**:1809–1821. DOI: https://doi.org/10.1016/j.celrep.2016.04.058, PMID: 27184841

Yang M, Yu H, Yu X, Liang S, Hu Y, Luo Y, Izsvák Z, Sun C, Wang J. 2022. Chemical-induced chromatin remodeling reprograms mouse ESCs to totipotent-like stem cells. *Cell Stem Cell* **29**:400–418. DOI: https://doi.org/10.1016/j.stem.2022.01.010, PMID: 35143761

Yu G, Wang LG, Han Y, He QY. 2012. clusterProfiler: an R package for comparing biological themes among gene clusters. *OMICS* **16**:284–287. DOI: https://doi.org/10.1089/omi.2011.0118, PMID: 22455463

Zhang X, Guo J, Wei X, Niu C, Jia M, Li Q, Meng D. 2018. Bach1: function, regulation, and involvement in disease. *Oxidative Medicine and Cellular Longevity* **2018**:1347969. DOI: https://doi.org/10.1155/2018/1347969, PMID: 30370001

Zhang Y, Huang Y, Dong Y, Liu X, Kou X, Zhao Y, Zhao A, Sun J, Su Z, Li Z, Zhang H, Li Y, Cao S, Wei J, Yin J, Kang L, Gao Y, Chen J, Wang Y, Li C, et al. 2021. Unique Patterns of H3K4me3 and H3K27me3 in 2-Cell-like Embryonic Stem Cells. *Stem Cell Reports* **16**:458–469. DOI: https://doi.org/10.1016/j.stemcr.2021.01.020, PMID: 33636112

Zhou W, Choi M, Margineantu D, Margaretha L, Hesson J, Cavanaugh C, Blau CA, Horwitz MS, Hockenbery D, Ware C, Ruohola-Baker H. 2012. HIF1α induced switch from bivalent to exclusively glycolytic metabolism during ESC-to-EpiSC/hESC transition. *The EMBO Journal* **31**:2103–2116. DOI: https://doi.org/10.1038/emboj.2012.71, PMID: 22446391

Zhu Y, Hon T, Ye W, Zhang L. 2002. Heme deficiency interferes with the Ras-mitogen-activated protein kinase signaling pathway and expression of a subset of neuronal genes. *Cell Growth & Differentiation* **13**:431–439 PMID: 12354752.